

# 3



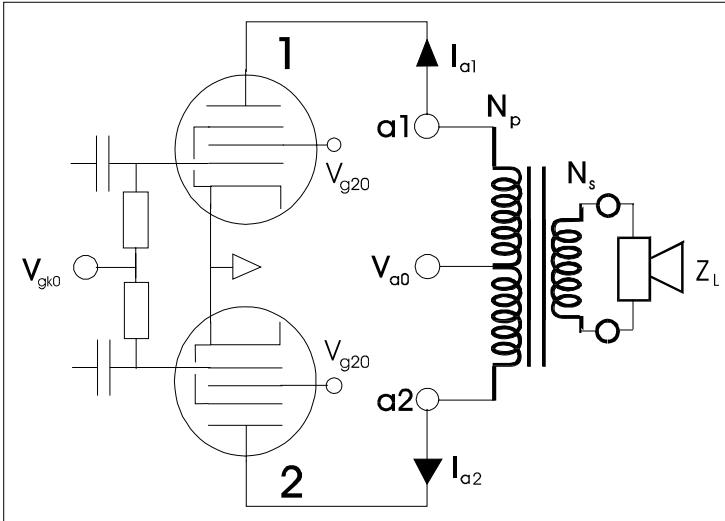
## Special coupling techniques between the valves and the transformer

In the previous chapters we have explored three coupling and driving techniques of the power valves and the output transformer. These were the single ended (SE) setup, the push-pull setup of triodes and pentodes, and the driven screen grid setup with a constant voltage supply to the control grid with anode coupling of the power valve to the output transformer.

There are, of course, more possible configurations of connecting an output valve to the transformer and some examples of these are: ultra-linear coupling, the cathode negative feedback and the cathode follower with the 'Unity Coupled' technique. The intention of this chapter is to discuss special coupling techniques and to introduce the new 'Super-Pentode<sup>®</sup>' setup. In the first part of this chapter general mathematical models will be formulated and subsequently these models will be applied to the various coupling techniques. Theoretical outcomes will be compared to measurements. The chapter will be concluded with an appendix whereby specifically designed toroidal output-transformers (the *Specialist*-range) will be introduced in order to realize the theoretical coupling techniques in practical setups.

### 3.1 | The general coupling model

The circuit of the power output part of a standard push-pull configuration is represented in figure 3.1.1. The centre tap of the output transformer has been connected to the power supply with the voltage  $V_{a0}$ ; the screen grids have a constant voltage  $V_{g20}$  and the control grids are connected to a negative voltage  $V_{g10}$ , with the aid of a high impedance control grid resistor. At rest (i.e. without an input signal applied) the anode of the power valves will conduct a current  $I_{a0}$ . The primary winding of the output transformer has a total of  $N_p$  windings and through the transformation of the secondary load impedance  $Z_L$ , the primary side has an impedance of  $Z_{aa}$ . The upper valve of the circuit will be valve-1 and the lower valve will be valve-2.



↑ **Figure 3.1.1** The standard pentode push-pull configuration.

For the realisation of alternative coupling methods between the power valves and the output transformer, special taps are needed on the primary or secondary windings, or additional windings must be wound on the output transformer. Figure 3.1.2 is an example of an output transformer with additional windings connected to the pentodes. There are two new windings added namely: a screen grid winding and a cathode winding.

It is not the case, however, that the circuits discussed can only be realised with this comprehensive transformer. However, this type of transformer makes it possible to formulate a universal model that can subsequently easily be adjusted to each type of circuit.

The centre tap of the new screen grid winding is connected to the supply voltage  $V_{g20}$ . The screen grid winding has  $N_{sch}$  windings and the ratio between  $N_{sch}$  and  $N_p$  equals  $x$ .

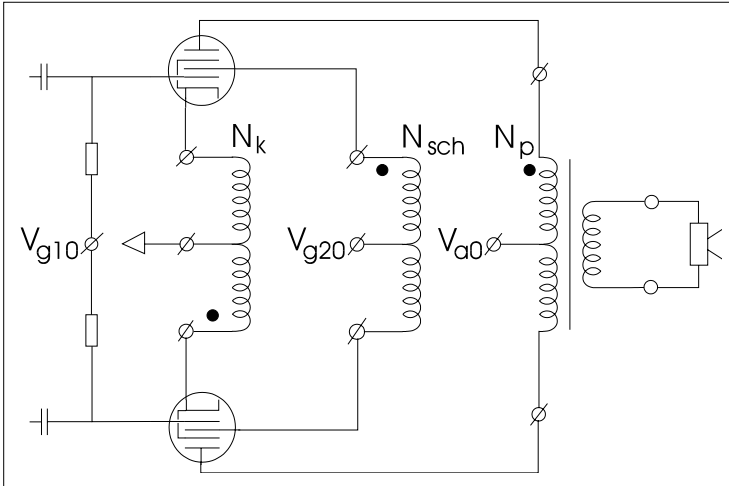
The cathode winding has a total of  $N_k$  windings and the ratio between  $N_k$  and  $N_p$  is represented by the symbol  $\Gamma$ .

$$x \frac{N_{sch}}{N_p} \quad \text{and} \quad \Gamma \frac{N_k}{N_p} \quad (3.1.1)$$

In figure 3.1.2 the equal phase-connection of each winding is indicated by the (fat) dot.

Suppose that the anode of valve-1 has a momentary voltage equal to  $V_{a1}$ . Then, over the top half of the primary winding a voltage change occurs that equals  $V_{a1} - V_{a0}$ . This voltage change is passed on by the transformer to the screen grid whereby the change of the screen grid voltage equals  $x \cdot (V_{a1} - V_{a0})$ .





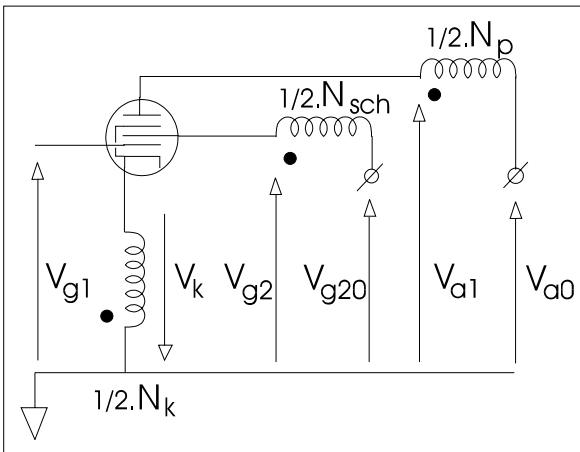
↑ **Figure 3.1.2** The general coupling model.

In the same manner the cathode voltage changes by  $-\Gamma \cdot (V_{a1} - V_{a0})$ . The minus sign is the result of the reverse voltage phase connection of the cathode negative feedback winding.

If the momentary driving voltage on the grid is  $V_{g1}$ , then the voltage between the control grid and the cathode is not equal to  $V_{g1}$ , but equals  $V_{g1k} = V_{g1} - V_k = V_{in} - (-\Gamma \cdot (V_{a1} - V_{a0}))$ .

Figure 3.1.3 gives an overview of the above voltages that occur in the schematic of figure 3.1.2.

When put into a formulaic format the voltages between the elements of valve-1 are as follows:



↑ **Figure 3.1.3** The definition of the voltages in valve-1.



$$\begin{aligned}
 V_{g1\ 1} &= V_{g10} + \Delta V \\
 V_{k\ 1} &= \Gamma \cdot V_{a1} - V_{a0} \\
 V_{g1k\ 1} &= V_{g1\ 1} - \Gamma \cdot V_{a1} - V_{a0} \\
 V_{g2\ 1} &= V_{g20} - x \cdot V_{a1} - V_{a0} \\
 V_{g2k\ 1} &= V_{g20} - x \cdot \Gamma \cdot V_{a1} - V_{a0} \\
 V_{ak\ 1} &= V_{a1} - \Gamma \cdot V_{a1} - V_{a0}
 \end{aligned} \tag{3.1.2}$$

In the formula of  $V_{g1}$ , a new voltage  $\Delta V$  is introduced, which represents the alternating voltage that is presented (in phase and in the opposite phase) to both the control grids in order to be amplified.

For the bottom valve-2, the same system of voltage equations can be prepared. With regards to driving the grid of valve-2 in the opposite phase, the alternating voltage equals  $-\Delta V$ .

If anode-1 has a voltage of  $V_{a1}$  then the anode-2 voltage will be  $(2 \cdot V_{a0} - V_{a1})$ . The voltage change of anode-2 is then  $(2 \cdot V_{a0} - V_{a1}) - V_{a0} = V_{a0} - V_{a1}$ . This is equal to the voltage change of anode-1, but opposite in sign.

Formula 3.1.3 shows the overview of the momentary voltages of valve-2.

$$\begin{aligned}
 V_{g1\ 2} &= V_{g10} - \Delta V \\
 V_{k\ 2} &= \Gamma \cdot V_{a0} - V_{a1} \\
 V_{g1k\ 2} &= V_{g1\ 2} - \Gamma \cdot V_{a0} - V_{a1} \\
 V_{g2\ 2} &= V_{g20} + x \cdot V_{a0} - V_{a1} \\
 V_{g2k\ 2} &= V_{g20} + x \cdot \Gamma \cdot V_{a0} - V_{a1} \\
 V_{ak\ 2} &= 2 \cdot V_{a0} - V_{a1} - \Gamma \cdot V_{a0} - V_{a1}
 \end{aligned} \tag{3.1.3}$$

In paragraph 1.14, the customised Child-Langmuir equation for pentodes is introduced where the voltages in that equation are considered in respect to the cathode. With the aid of formulas 3.1.2 and 3.1.3 the anode currents  $I_{a1}$  and  $I_{a2}$  can be calculated for each value of  $V_{g10}$ ,  $V_{g20}$ ,  $V_{a0}$ ,  $\Delta V$ ,  $x$  and  $\Gamma$ . If one gives  $j$  the value of 1 or 2, in order to indicate with this either valve-1 or valve-2, then the respective anode currents are as follows:



$$\alpha_j = \alpha_0 \frac{2}{\pi} \arctan \frac{V_{akj}^{\frac{1}{n}}}{V_{g2kj}} \quad (3.1.4)$$

$$I_{aj} = \alpha_j K V_{g1kj} D_{g2} V_{g2kj} D_a V_{akj}^{\frac{3}{2}}$$

Subsequently the screen grid and cathode currents can be calculated with the aid of 3.1.5 and 3.1.6.

$$I_{g2j} = \frac{1 - \alpha_j}{\alpha_j} I_{aj} \quad (3.1.5)$$

$$I_{kj} = I_{aj} - I_{g2j} \quad (3.1.6)$$

Each of the currents, as calculated with the aid of formulas 3.1.4, 3.1.5 and 3.1.6 creates within the output transformer a flux density. The sum of the separate flux densities is equal to the total flux density which is generated by the currents of valve-1 within the core of the output transformer. Please note that these flux densities are aligned by the current and phase direction of the windings.

$$\begin{aligned} B_{a1} &= \frac{\mu_0 \mu_r}{l_{eff}} \frac{1}{2} N_p I_{a1} \\ B_{g21} &= \frac{\mu_0 \mu_r}{l_{eff}} \times \frac{1}{2} N_p I_{g21} \\ B_{k1} &= \frac{\mu_0 \mu_r}{l_{eff}} \Gamma \frac{1}{2} N_p I_{k1} \\ B_{tot1} &= B_{a1} + B_{g21} + B_{k1} \end{aligned} \quad (3.1.7)$$

In these formulas of the flux densities the terms used have the following meaning:  $\mu_0$  is the magnetic permeability of the vacuum;  $\mu_r$  is the relative magnetic permeability of the core material; and  $l_{eff}$  is the effective length of the core of the output transformer, measured along the average distance path of the magnetic field lines within the core. The current,  $I_{a-1}$ , flows through the  $1/2 \cdot N_p$  windings.  $I_{g2-1}$  flows through  $x \cdot 1/2 \cdot N_p$  windings and  $I_{k-1}$  through  $\Gamma \cdot 1/2 \cdot N_p$  windings.

$I_{a-1}$ ,  $I_{g2-1}$ , and  $I_{k-1}$  are interrelated as shown by the formulas 3.1.5 and 3.1.6. The completion of this in formula 3.1.7 gives us:

$$B_{tot1} = \frac{\mu_0 \mu_r 0,5 N_p}{l_{eff}} I_{a1} \left( 1 - \frac{x}{\alpha_1} \right) + \frac{\Gamma}{\alpha_1} I_{a1} \quad (3.1.8)$$



This means that the upper half of the primary winding is driven by an effective current  $I_{\text{eff-1}}$  (see formula 3.1.9).

The same reasoning is also valid for the effective current that is supplied by valve-2 to the bottom part of the primary winding.

$$I_{\text{eff } j} = I_{a j} \cdot \frac{1}{\alpha_j} = \frac{\Gamma}{\alpha_j} \quad (3.1.9)$$

Each of the two power valves can now be understood to be a current source that delivers  $I_{\text{eff-j}}$  in parallel with an internal resistance  $r_{i-j}$  which is represented by formula 3.1.10:

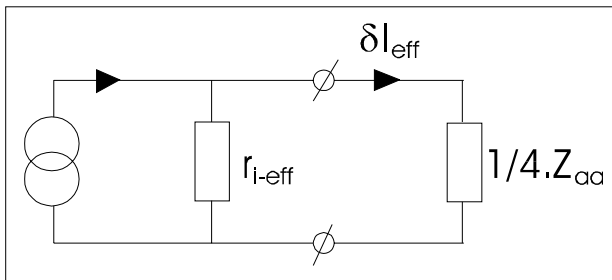
$$r_{i j} = \frac{\partial I_{\text{eff } j}}{\partial V_{a j}} \quad (3.1.10)$$

These two current sources together form one effective current source  $\delta I_{\text{eff}}$ , which is equal to the difference of the two currents of formula 3.1.9. For this please refer to paragraph 2.6. Connected to this effective current source are the two internal resistances of formula 3.1.10 in parallel (formulas 3.1.11 and 3.1.12).

$$\delta I_{\text{eff}} = I_{\text{eff } 1} - I_{\text{eff } 2} \quad (3.1.11)$$

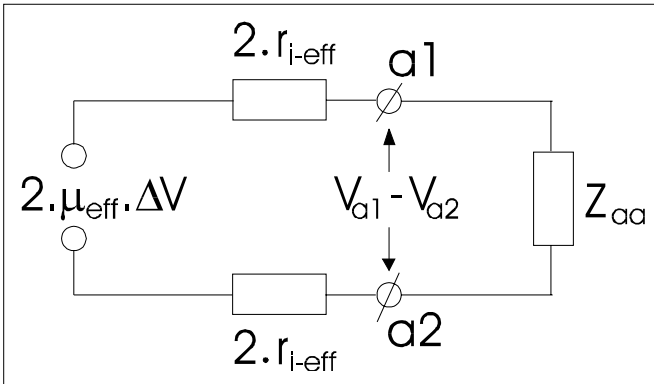
$$r_{i \text{ eff}} = \frac{1}{\frac{1}{r_{i 1}} + \frac{1}{r_{i 2}}} \quad (3.1.12)$$

In paragraph 2.6 we also saw that the resultant effective current source drives a primary impedance of  $1/4 \cdot Z_{aa}$ . With the aid of the above deliberations, a complete current source replacement model of the push-pull configuration can be created as represented in figure 3.1.4. Figure 3.1.5 shows the equivalent circuit whereby the push-pull circuit has been represented by an equivalent voltage source.



↑ **Figure 3.1.4** The complete push-pull circuit is here substituted by a current source delivering  $\delta I_{\text{eff}}$  into  $1/4 \cdot Z_{aa}$ .





↑ **Figure 3.1.5** The complete push-pull circuit is here substituted by a voltage source delivering  $(V_{a1} - V_{a2})$  over  $Z_{aa}$ .

The introduced term  $\mu_{\text{eff}}$  gives expression to the fact that the alternating voltage between the control grids of the power valves is amplified enough to create an alternating voltage of the value  $(V_{a1} - V_{a2})$  between the anode connections a1 and a2. The relationship between  $\mu_{\text{eff}}$  and the different voltages, currents and valve parameters will not be further elaborated upon.

A final remark on this coupling model: the current model of figure 3.1.4 replaces the complete output transformer with a new transformer with the primary having  $1/2 \cdot N_p$  windings and the secondary  $N_s$  windings. By using the derived  $r_{i\text{-eff}}$  values the damping factor of the secondary winding can be calculated. Both the models shown above will give the same results.

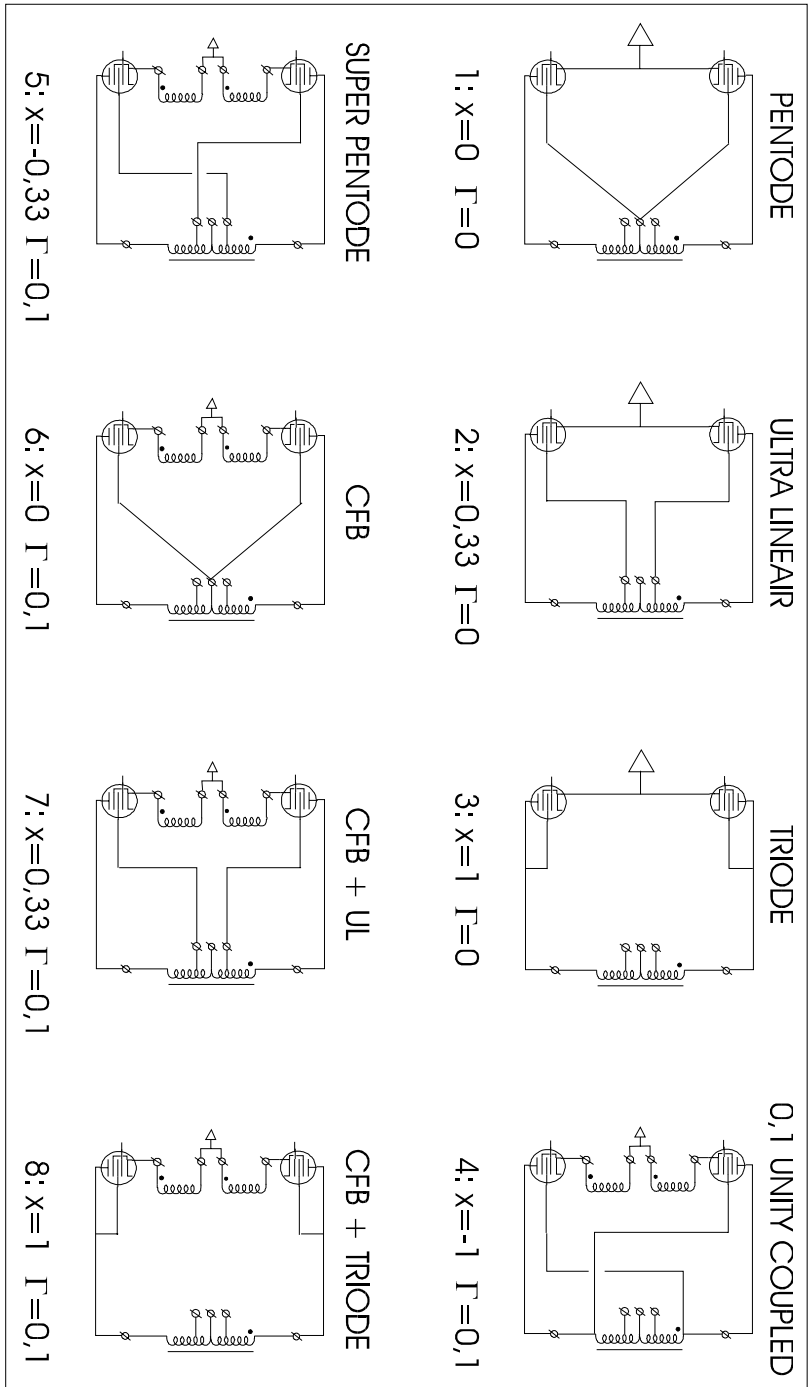
### 3.2 | Testing the coupling model

The defined coupling model (paragraph 3.1) has been tested with the aid of two EL34 power valves in push-pull amplifier configurations whereby the valves receive a  $V_{a0} = 450$  V and each having an idling current of 45 mA. The toroidal output transformer used was the VDV-2100-CFB/H (= PAT-2100-CFB/H), with the secondary loaded with 8  $\Omega$ .

On this transformer additional windings are present for use with the special cathode and screen grid connections, with the respective  $x$  and  $\Gamma$  values (see figure 3.2.1). The winding ratio  $N_p/N_s$  from the anodes to the load is 20.

The internal resistance  $R_{ip}$  of the primary winding is 56  $\Omega$ . The internal resistance  $R_{is}$  of the secondary winding is equal to 0.10  $\Omega$ . This means that the primary winding has a total impedance of  $Z_{aa} = 56 + 20^2 \times (8 + 0.1) = 3296$   $\Omega$ .

The maximum output power (on the verge of clipping) was measured, over the secondary 8  $\Omega$  load, for each configuration with a 1 kHz alternating voltage.



↑ **Figure 3.2.1** The power valve/output transformer configurations for the testing of the coupling model of paragraph 3.1.



As a result of the internal resistances of the primary and secondary windings an *insertion loss* arises within the transformer.

The power effectively developed in the 8 Ω load resistor is  $8/(8 + 0.1 + 20^{-2} \cdot 56) = 97\%$  of the effective power delivered by the power valves. The calculations of the output power are made to compensate for this loss.

By a minimal output voltage (10 mW into 8 Ω) the output impedance of each amplifier was determined and transformed back to the primary of the output transformer. This is equal to  $4 \cdot r_{i\text{-eff}}$  (see figure 3.1.5) so that with this  $r_{i\text{-eff}}$  could be determined.

Figure 3.2.1 gives an overview of the circuits used.

In the test amplifiers EL34 power valves, that were burned in for several hours, were used. As this process has an influence on the parameters of the respective valves they were measured again for the  $V_{g1k} = 0$  V-line, as these are determinative of the maximum output power. This resulted in the following 'older-valve' parameters:

$$[n; \alpha_0; K; D_a; D_{g2k}] = [5; 0,992; 2,188 \cdot 10^{-3}; 2,343 \cdot 10^{-3}; 96,5 \cdot 10^{-3}]$$

In comparison with the parameters given in chapter 1 it is especially striking that the  $D_a$  value has changed. The output powers were calculated using these 'older valve' parameters and the output powers were measured (error measurement  $\pm 7\%$ ). They are in excellent agreement. See tables 3.2.1 and 3.2.2 below.

Subsequently other characteristics were obtained in detail at the set operating point. This resulted in:  $S = 4.53$  mA/V and  $r_{i\text{-eff}} = 15700$  Ω by a  $V_{a0} = 450$  V and  $I_{a0} = 45$  mA / valve (pentode setup).

**Table 3.2.1: CALCULATED output power and  $r_{i\text{-eff}}$  for the circuits of figure 3.2.1**

<i>circuit</i>	1	2	3	4	5	6	7	8	<i>dimension</i>
$P_{\max}$ (1)	74	55	27	/	78	72	53	26	W
$r_{i\text{-eff}}$ (2)	15700	2541	844	/	1239	842	622	387	Ω

(1): insertion los of 3 % is included in the calculation;

(2): with  $S = 4.53$  mA/V and  $r_{i\text{-eff}} = 15,700$  Ω by a  $V_{a0} = 450$  V and  $I_{a0} = 45$  mA.

**Table 3.2.2: MEASURED output power and  $r_{i\text{-eff}}$  for the circuits of figure 3.2.1**

<i>circuit</i>	1	2	3	4	5	6	7	8	<i>dimension</i>
$P_{\max}$ (3)	74	55	27	/	80	63	49	27	W
$r_{i\text{-eff}}$ (4)	15700	2390	840	/	1230	830	610	400	Ω

(3): maximum output power into an 8 Ω load resistor;

(4): measured by a 10 mW output power in to 8 Ω.



With the aid of the above data the values of  $r_{i\text{-eff}}$  for circuit 2 to 8 are calculated. The parity between measurements and calculations are shown in tables 3.2.1 and 3.2.2.

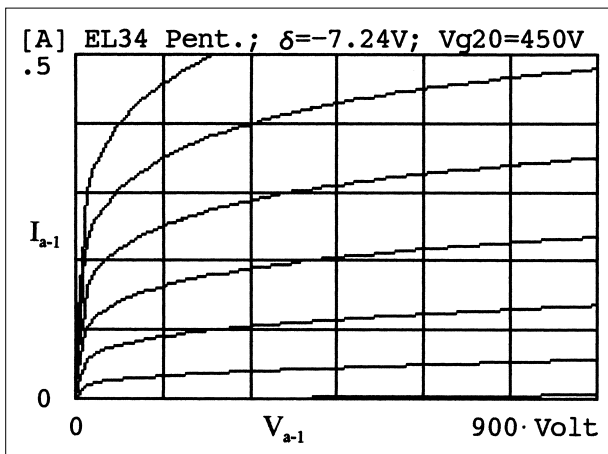
In the subsequent paragraphs, with the aid of calculations, the circuits of figure 3.2.1 are explored in detail. As mentioned above these calculations are based upon using the 'old-valve' values as these describe the used EL34 power valves very well. They show only a divergence for the calculations of  $r_{i\text{-eff}}$  (a maximum of factor 2) to the measured values. This is the reason why  $r_{i\text{-eff}}$  is calculated with the characteristics determined around the operating point, which will ensure that very accurate  $r_{i\text{-eff}}$  values are obtained.

### 3.3 | Pentode based push-pull power amplifier

Figure 3.2.1-1 shows the standard pentode push-pull amplifier where the anodes are connected directly to the output transformer, the screen grids receive a constant supply voltage and the idling current has been set via a negative control grid voltage  $V_{g10}$ .

For the anode idling current  $I_{a0} = 45 \text{ mA}$  at  $V_{a0} = V_{g20} = 450 \text{ V}$ , the calculation according to formula 3.1.4 shows that the control grids of both the power valves should receive a negative voltage of  $V_{g10} = -36.2 \text{ V}$  ( $-37 \text{ V}$  according to the measurement). The minor discrepancy between the measurement and the calculation is ignored.

With the aid of formula 3.1.4 the characteristics of the power valves have been calculated, where  $V_{ak}$  varies from 0 to  $2 \cdot V_{a0} = 900 \text{ V}$ . The  $V_{g1k}$  value changes in 10 steps from 0 V to  $-2 \cdot V_{g10} = -72.4 \text{ V}$ . These are the limit values of the grid voltages, whereby the grids have been driven to the point where the grid current just not flows. In the notations given in the previous chapters this means  $\delta$

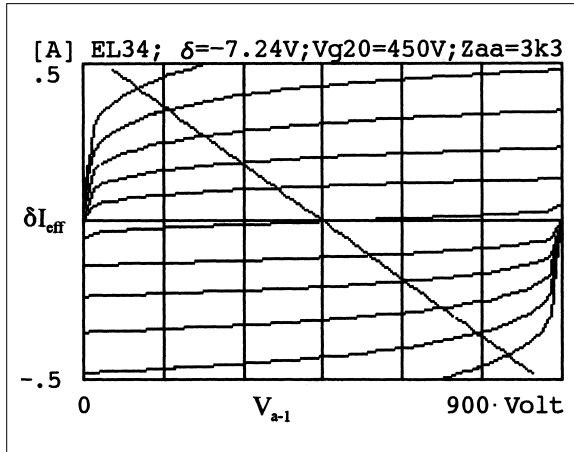


↑ **Figure 3.3.1** The  $I_a/V_{ak}/V_{g1k}$ -characteristics of the EL34.



equals  $-72.4/10 = -7.24$ , the fifth characteristic line represents the idling of the power valves (calculated from the left characteristic line where  $V_{gk} = 0$  V).

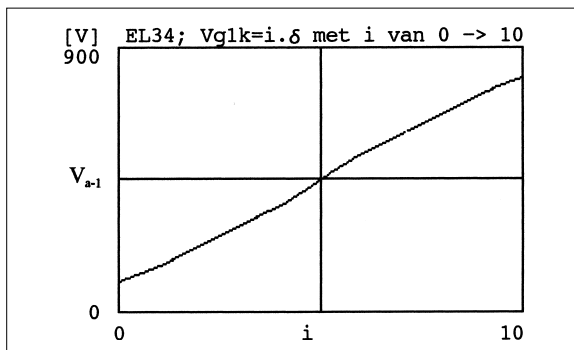
The current  $\delta I_{eff}$  that drives the output transformer is given by formula 3.1.11 and this is calculated by placing the corresponding characteristics of the power valves below one another and subtracting from each other. Figure 3.3.2 shows these  $\delta I_{eff}$  characteristics, while the load line of the output transformer ( $1/4 \cdot Z_{aa}$ ) has also been drawn in.



↑ **Figure 3.3.2**  $\delta I_{eff} = I_{a-1} - I_{a-2}$  and  $1/4 \cdot Z_{aa}$ .

Via an iterative calculations process the crossing points of the  $\delta I_{eff}$ -lines with the  $1/4 \cdot Z_{aa}$ -lines are subsequently determined. This delivered per valve the coupled values of the anode voltages, together with the respective grid voltages, the respective anode currents and the respective screen grid currents.

Figure 3.3.3 shows the first result, the horizontal axis represents the control grid voltage ( $V_{g1k} = \delta \cdot i$  with  $i$  from 0 to 10) and the vertical axis is the respective anode voltage.



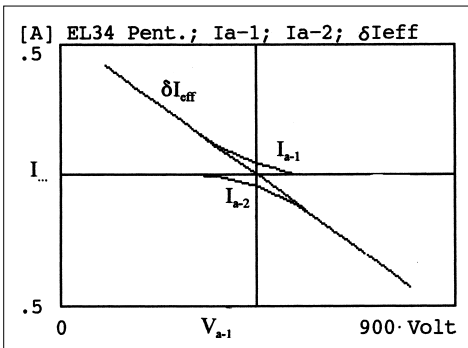
↑ **Figure 3.3.3**  $V_{a-1}$  as function of  $V_{g1k} = \delta \cdot i$ .



This figure is often shown when testing valve amplifiers on the oscilloscope screen, the X-axis of the oscilloscope shows the control grid voltage and the Y-axis the anode voltage. The straighter the line the less distortion the (no negative feedback) amplifier produces. In the case of this pentode based push-pull amplifier it is clearly visible that in the middle of the graph (around the point of idling) the slopes of the graph are steeper than at the ends of the line. Some of the distortion produced by the power amplifier is already visible here.

At the same time we have available the anode currents of both the power valves as function of the respective anode voltages. These are shown in figure 3.3.4 where, at the same time, the effective current  $\delta I_{\text{eff}}$  has been shown. In the graph it is clearly visible that around the area of the operating point the pentode based power amplifier operates within class-A.

When the power valves are increasingly driven harder they will switch off alternately. This happens when the anode voltage is larger than 582 V. The class-A output power is therefore 10.6 W (formula 2.6.3, re-written to  $P = 2 \cdot \delta V_{a1}^2 / Z_{aa}$  with  $\delta V_{a1} = 582 - 450$  V). With a larger output power the amplifier will move into class-B.

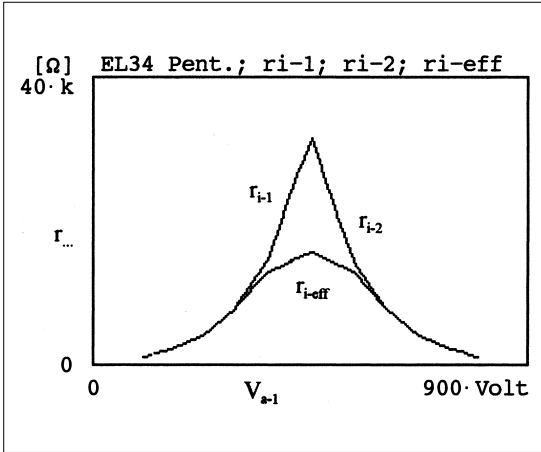


↑ **Figure 3.3.4**  $I_{a-1}$ ,  $I_{a-2}$  and  $\delta I_{\text{eff}}$  as function of  $V_{a-1}$ .

Figure 3.3.5 shows the behaviour of the internal resistances of the power valves, calculated with formulas 3.1.10 and 3.1.12. Within this figure three lines are visible. The top lines are the internal resistances,  $r_i$ , per power valve (formula 3.1.10) while the lower curves belong to  $r_{i-\text{eff}}$ . Within this graph it is clearly visible that the power valves switch off in an alternate fashion whereby the internal resistance increases to a very large value. The conducting valve will then take over the driving of the output transformer and its  $r_{i-\text{eff}}$  is equal to the internal resistance of the conducting valve.

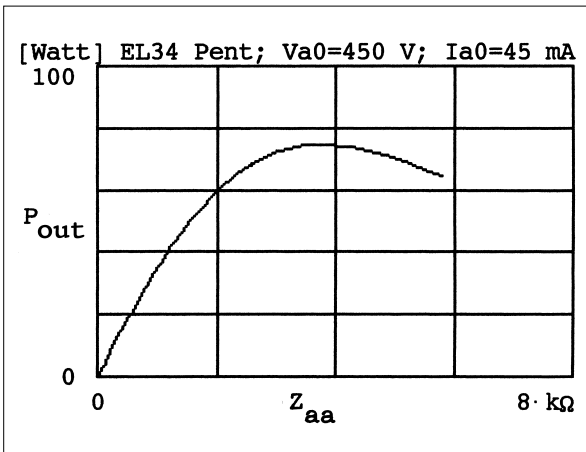
The output transformer sees effectively  $r_{i-\text{eff}}$ , the calculations show that this value is not a constant and in some cases even, when driven to its maximum, (in this specific case) actually decreases. This then will give rise to two remarks:





↑ **Figure 3.3.5** Internal resistances as function of  $V_{a-1}$ .

- a The variation of  $r_{i-eff}$  as a function of the output power explains why some amplifiers with negative feedback have a tendency to oscillate when driven closer to their maximum (or closer to their minimum). The output transformer shows, in combination with the changed value of  $r_{i-eff}$ , a different open-loop bandwidth, that may result in oscillation in the amplifier with negative feedback.
- b Some people claim that they can hear the change over from class-A to class-B. Assuming the fact that  $r_{i-eff}$  determines the damping factor of the (no negative feedback) amplifier, it is clear that the damping of the loudspeakers, as a function of the output power changes. This can give rise to audible changes in the frequency characteristics of the amplifier and the loudspeaker combined.



↑ **Figure 3.3.6**  $P_{out}$  as function of  $Z_{aa}$ .



It also shows that the damping factor as a function of the momentary output signal, changes dynamically. That this has an influence upon the sound reproduction, speaks for itself.

Lastly figure 3.3.6 shows the output power as function of  $Z_{aa}$  (see chapter 2.7).

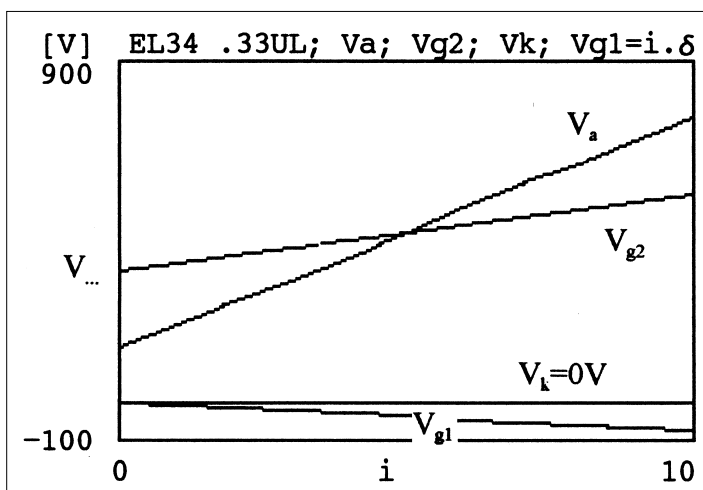
### 3.4 | The ultra-linear push-pull power amplifier

In the second power amplifier circuit of figure 3.2.1 the screen grids of the EL34 power valves are connected to the taps of the primary winding. The placement of the taps is chosen in such a way that 33 % of the anode voltage variations are delivered into the screen grid.

Whether these screen couplings are realised with the aid of an independent winding, or as taps on the primary winding, as in the case here, has no influence upon the coupling theory of paragraph 3.1. It is just the case that  $V_{a0} = V_{g20}$ , so when at rest both the screen grid and the anode have an equal voltage.

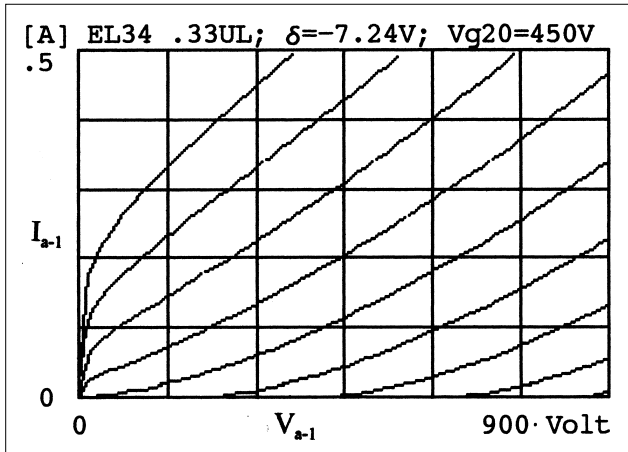
Figure 3.4.1 shows the voltages of the anode, the screen grid, the cathode and the control grid of valve-1. In the middle of this graph, at  $i = 5$  is the control grid voltage  $-36.2$  V. This is the idling position and for  $V_{a0} = V_{g20} = 450$  V. From  $-36.2$  V  $V_{g1k}$  varies from 0 to  $-72.4$  V. The result is that both the anode- and screen grid-voltages are subjected to change. It is clearly visible that the screen grid voltage variation is one third of the anode voltage variation.

With the aid of formula 3.1.2 ( $x = 0.33$  and  $\Gamma = 0$ ) and formula 3.1.4 we can now calculate the  $I_a/V_{ak}/V_{g1k}$ -characteristics whereby  $V_{g1k}$  in 10 steps varies from 0 to  $10 \cdot \delta$  ( $\delta = -7.24$  V). Figure 3.4.2 shows the result.



↑ **Figure 3.4.1** The valve voltages in a UL-configuration.



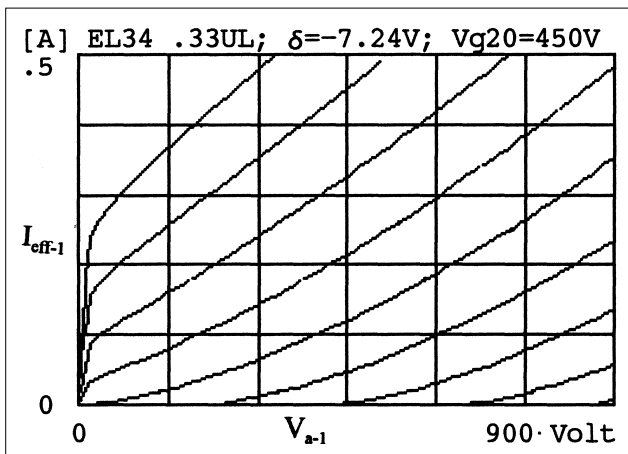


↑ **Figure 3.4.2** The UL anode current characteristics.

It is clearly visible that the curves, because of the screen grid negative feedback, have a steeper slope, which is synonymous with a lower internal valve resistance.

The output transformer is not only driven by the anode current flowing through the primary winding; the screen grid also drives a part of this winding by the virtue of its output current and therefore also plays its part in the flux density of the output transformer. This is expressed by formula 3.1.9. In this, the effective current  $I_{eff}$  per valve is determined and the characteristics of this are represented in figure 3.4.3. The comparison of the figures 3.4.2 and 3.4.3 clearly shows that the  $I_{eff}$ -lines are higher than the  $I_a$ -lines.

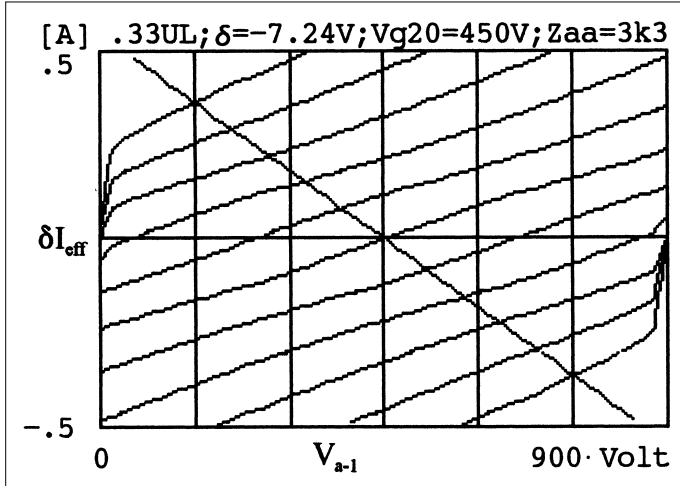
The difference  $\delta I_{eff}$  of the effective currents of the power valves drives half the primary winding. The characteristics plus the associated  $1/4 \cdot Z_{aa}$  load line can



↑ **Figure 3.4.3** The effective current characteristics.

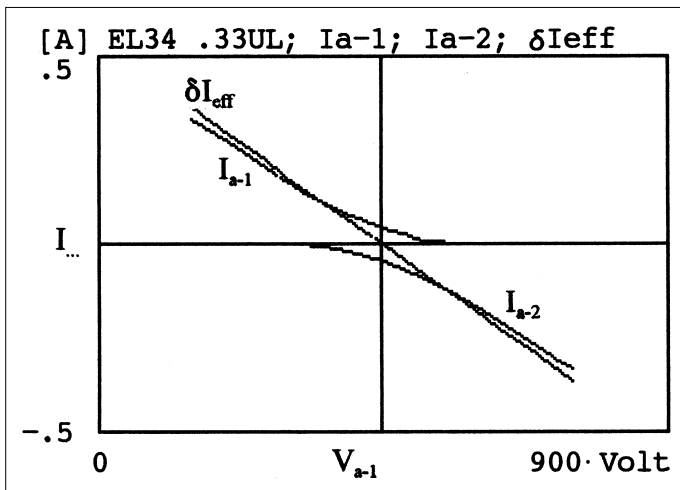


be found in figure 3.4.4. The intersections of the lines in figure 3.4.4, gives the coupled values of the anode and the screen grid voltages as a function of the control grid voltage. These intersections were already used by the creation of figure 3.4.1. In that graph it is visible that the anode voltage varies in a more linear fashion with the control grid than in the pentode configuration of paragraph 3.3. The negative feedback via the screen grid ensures a lower distortion.



↑ Figure 3.4.4  $\delta I_{eff} = I_{a-1} - I_{a-2}$  and  $1/4 \cdot Z_{aa}$ .

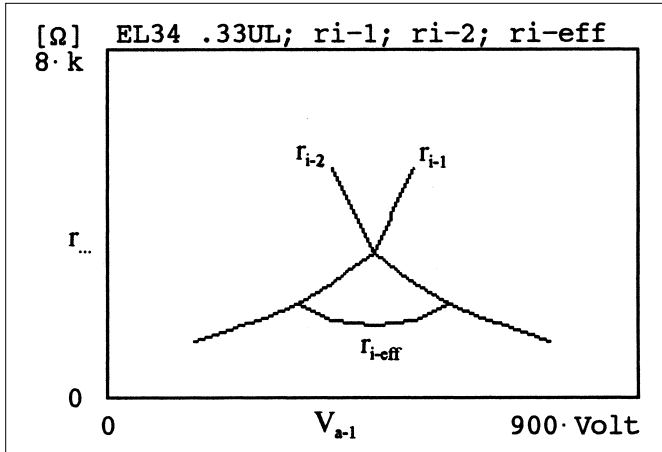
In figure 3.4.5 the anode currents  $I_{a-1}$  and  $I_{a-2}$  and the effective difference current  $\delta I_{eff}$  are represented as a function of the anode voltage of valve-1. The changeover from class-A into class-B is clearly visible. It is noticeable that  $\delta I_{eff}$  is



↑ Figure 3.4.5  $I_{a-1}$ ,  $I_{a-2}$  and  $\delta I_{eff}$  as function of  $V_{a-1}$ .

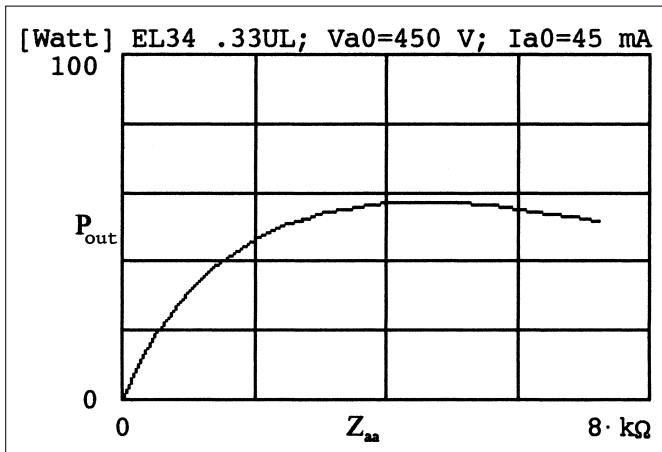


larger than the anode currents; the cause of this is again the influence of the screen grid currents. The behaviour of the internal valve resistances and  $r_{i-eff}$  is represented in figure 3.4.6 and here it is noticeable that  $r_{i-eff}$  remains more constant than in the pentode configuration of paragraph 3.3. The previously discussed variation of the dynamic damping factor is here significantly lower. Besides that the  $r_{i-eff}$  value as a result of the screen grid negative feedback is much smaller than in a pentode configuration, resulting in a drastically increased damping of the loudspeaker connected to the secondary winding.



↑ **Figure 3.4.6** The internal resistances as function of  $V_{a-1}$ .

In conclusion: by which  $Z_{aa}$ -value is the maximum output power obtained? Figure 3.4.7 gives the answer: at around  $Z_{aa} = 4500 \Omega$  will the maximum power be obtained (a little more than 55 W). If we compare the ultra-linear setup with



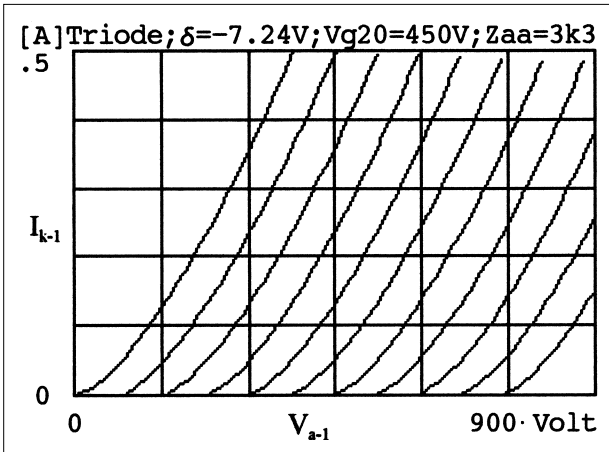
↑ **Figure 3.4.7**  $P_{out}$  as function of  $Z_{aa}$ .

the pentode configuration, then it is striking that the output power is somewhat reduced from 74 to 55 W. The loudspeaker damping factor, however, has increased sixfold, the harmonic and the intermodulation distortions have been reduced (this as a result of the linear dependency between  $V_{a-1}$  and  $V_{g1k}$ ), while the variation of the dynamic damping factor is also much reduced.

### 3.5 | Triode push-pull power amplifier

In circuit 3 of figure 3.2.1 the EL34 power valves are configured as triodes by connecting their screen grids with the anodes ( $x = 1$ ). In this situation separate calculations of the screen grid and anode currents are not required (unless the maximum dissipation must be known) and therefore the cathode current  $I_{k-j}$  is calculated as a function of the anode and screen grid voltages.

The combinations of formulae 3.1.4 to 3.1.6 and 3.1.9 show that the cathode currents  $I_{k-j}$  and the  $\alpha_j$ -term disappears and that  $I_{\text{eff}-j} = I_{k-j}$  becomes valid. Figure 3.5.1 shows the characteristics of these cathode currents; these have clearly the qualities of triode power valves.



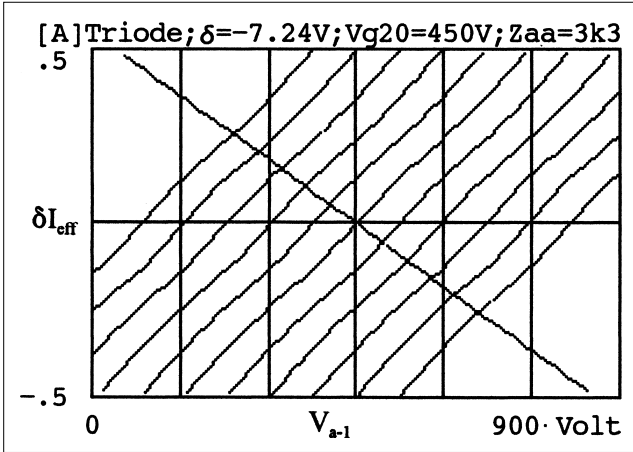
↑ **Figure 3.5.1** The triode-cathode current characteristics.

The characteristics of the difference current  $\delta I_{\text{eff}}$  that effectively drive the output transformer, are depicted in figure 3.5.2. In this figure the grid voltage varies in 10 steps of  $\delta = -7.24\text{ V}$ . The load line  $1/4 \cdot Z_{aa}$  has also been drawn in.

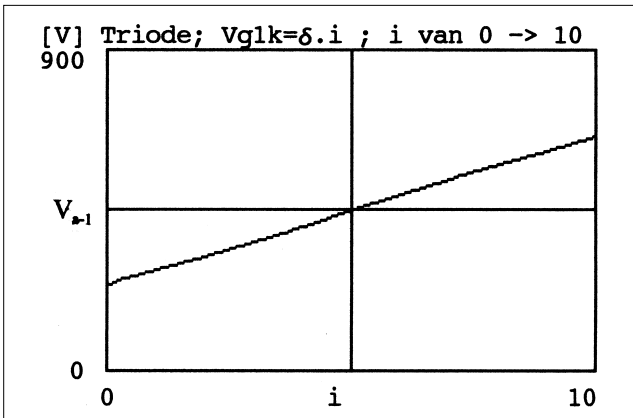
The figures 3.5.3, 3.5.4 and 3.5.5 show the  $V_{a-1}/V_{g1k}$ -linearity and the currents per valve, plus  $\delta I_{\text{eff}}$  and the internal resistances as function of  $V_{a-1}$ .

It is notable that in the above figures the linearity may be termed as being 'reasonable', while the variation of the dynamic damping factor is considerable.

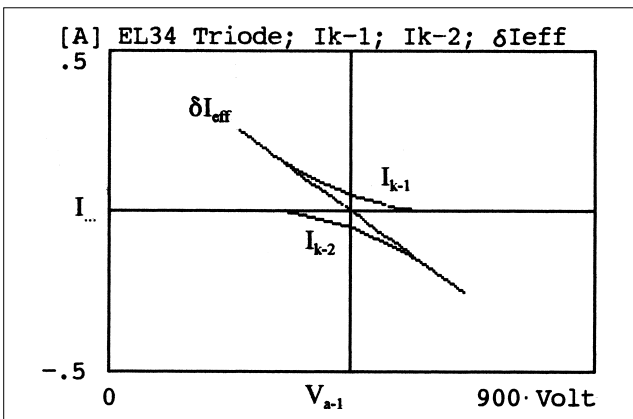
That is why in the next paragraph discussions will be had regarding the way that the properties of the triode push-pull can be improved upon. We shall do this



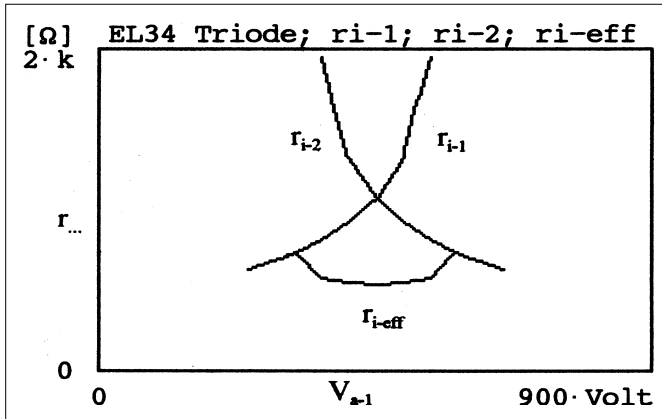
↑ **Figure 3.5.2**  $\delta I_{eff} = I_{k-1} - I_{k-2}$  and  $1/4 \cdot Z_{aa}$ .



↑ **Figure 3.5.3**  $V_{a-1}$  as a function of  $V_{g1k} = \delta \cdot i$ .



↑ **Figure 3.5.4**  $I_{a-1}$ ,  $I_{a-2}$  and  $\delta I_{eff}$  as a function of  $V_{a-1}$ .

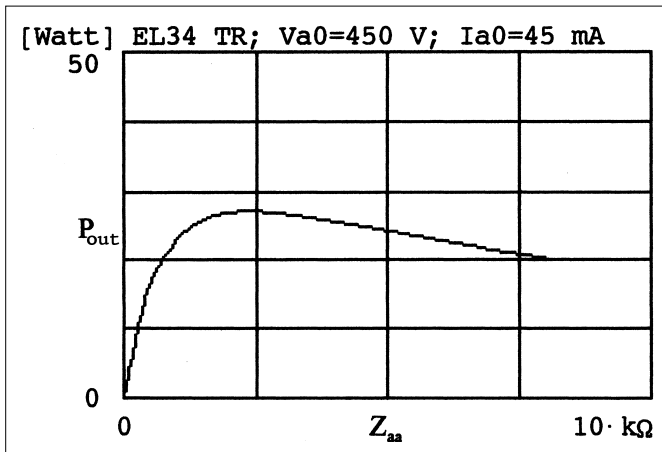


↑ **Figure 3.5.5** Internal resistances as function of  $V_{a-1}$ .

with the aid of the universal coupling technique, as discussed in the previous paragraphs, but additionally we shall delve deeper into the manner on how the coupling model can be used to optimally improve upon the properties of the amplifier.

### 3.6 | Optimising the triode push-pull amplifier

Figure 3.5.2 of the previous paragraph shows something interesting. Around the area where  $\delta I_{eff} = 0$  [A] the slopes of the characteristics are steeper than in the areas where  $\delta I_{eff}$  has a larger value (for  $|\delta I_{eff}| > 150$  mA). The  $1/4 \cdot Z_{aa}$ -line cuts this steeper line in the middle, but by a larger  $V_{a-1}$  voltage on the intersections the  $\delta I_{eff}$ -gradients are less steep. We may thus expect that the effective internal resistance  $r_{i-eff}$  will not be constant (see figure 3.5.5).



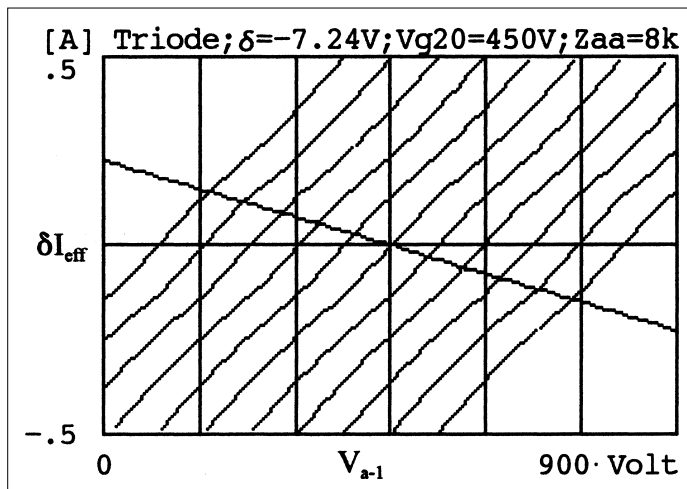
↑ **Figure 3.6.1**  $P_{out}$  as a function of  $Z_{aa}$ .



When one strives to get a more constant  $r_{i\text{-eff}}$  and a better  $V_{a-1}/V_{gk1}$ -linearity, then a larger  $Z_{aa}$  must be chosen so that at the  $V_{gk1} = 0$  V border line values, the intersections of the  $Z_{aa}$  line with the  $\delta I_{\text{eff}}$  -characteristics, still falls just within the area of the steeper slopes. This, however, is to the detriment of the output power (see figure 3.6.1) but prevents the variation of the dynamic damping factor and, as will be shown later on, improves the linearity considerably.

Instead of an anode load of  $Z_{aa} = 3.3 \text{ k}\Omega$ , an output transformer with a larger  $N_p/N_s$  windings ratio is therefore used – as, for instance, the toroidal output transformer VDV8020 (= PAT-1080PP) with  $N_p/N_s = 40$ . If this transformer will be loaded on the secondary with a loudspeaker impedance of  $5 \Omega$ , then  $Z_{aa}$  is  $8 \text{ k}\Omega$ .

In figure 3.6.2 this load line has been drawn into the  $\delta I_{\text{eff}}$  characteristics. When driven to its maximum, the load line intersects with the steeper parts of the  $\delta I_{\text{eff}}$  characteristics.

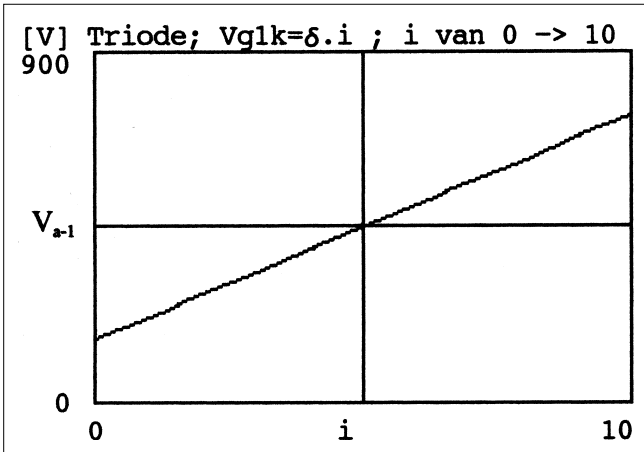


↑ **Figure 3.6.2**  $\delta I_{\text{eff}} = I_{k1} - I_{k2}$  and  $1/4 \cdot Z_{aa}$  with  $Z_{aa} = 8 \text{ k}\Omega$ .

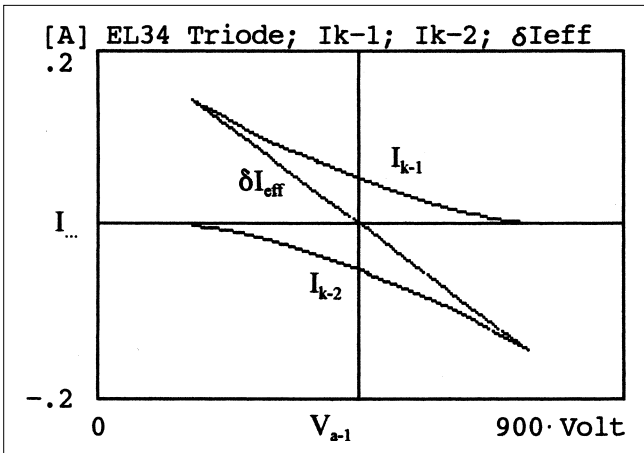
Iterative calculations of the intersections gives a remarkable number of details.

Figure 3.6.3 shows the first result. The anode voltages change in a linear fashion with the control grid voltages and the kink around the centre, as shown in figure 3.5.3 (use a ruler) has now completely disappeared. This means a hefty reduction in distortion.

The second result is even more remarkable. In figure 3.6.4 the valve currents have been calculated. The graph of the valve currents shows clearly that this triode push-pull amplifier, even when driven to its maximum, works completely in class-A. The output power within this setup is a little more than 20 W (20.5 W to be precise), which is also something that can be made out in figure 3.6.1.



↑ **Figure 3.6.3**  $V_{a-1}$  as a function of  $V_{g1k} = \delta \cdot i$  with  $Z_{aa} = 8 \text{ k}\Omega$ .



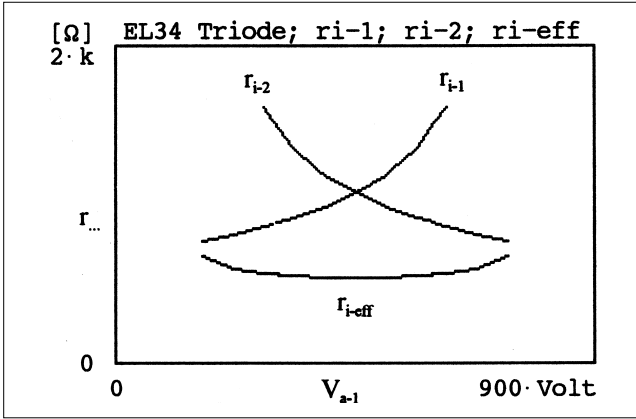
↑ **Figure 3.6.4**  $I_{a-1}$ ,  $I_{a-2}$ ,  $\delta I_{eff}$  with  $Z_{aa} = 8 \text{ k}\Omega$ .

Figure 3.6.5 shows the behaviour of the internal resistances of the valves. Again it is visible that these resistances have a more constant value as a function of the driving range.

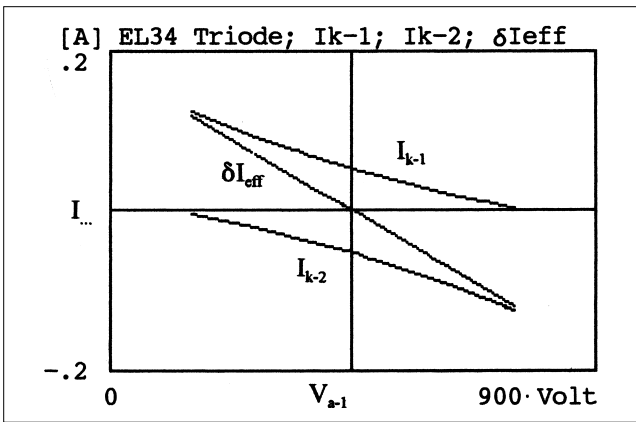
The results of the calculations with the coupling model of this triode based amplifier can be summarised as follows:

Based on the calculated  $\delta I_{eff}$ -characteristics an optimum  $Z_{aa}$  load line can be found, where the mutual distances of the intersections of  $Z_{aa}$  load line with  $\delta I_{eff}$  remain as constant as possible. With this the linearity between the anode and the control grid voltages has been optimised. Based on the slopes of the  $\delta I_{eff}$ -characteristics a  $Z_{aa}$  load line can be defined, where the  $\delta I_{eff}$ -slopes in the intersections remain as constant as possible. This procedure minimises the variations of the dynamic damping factor.

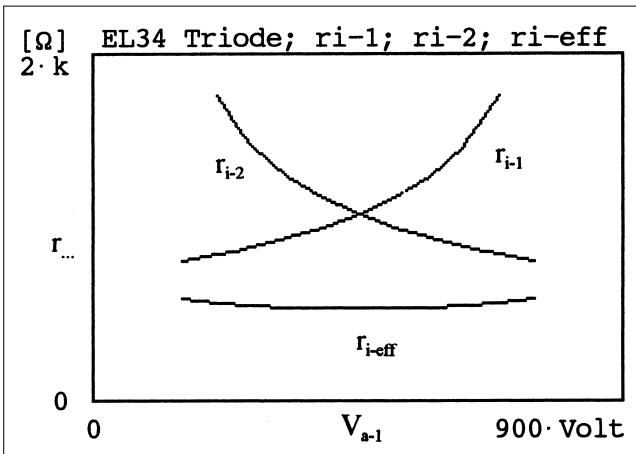




↑ **Figure 3.6.5** Internal valve resistances;  $Z_{aa} = 8 \text{ k}\Omega$ .



↑ **Figure 3.6.6**  $I_{a-1}$ ,  $I_{a-2}$ ,  $\delta I_{eff}$  with  $Z_{aa} = 10 \text{ k}\Omega$ .



↑ **Figure 3.6.7** Internal valve resistances;  $Z_{aa} = 10 \text{ k}\Omega$ .



These techniques show how important it is to have knowledge of the  $\delta I_{\text{eff}}$  characteristics in order to ensure as optimum as possible the power amplifier settings.

In conclusion, as a nice exercise, this triode push-pull amplifier is also re-calculated with a  $Z_{\text{aa}}$  value of 10 k $\Omega$ . When subjected to this load and when driven to its maximum this amplifier will remain firmly in class-A (see figure 3.6.6). However, in regards to the efficiency settings this is not the best choice, but as figure 3.6.7 shows the variation in the damping factor has been reduced even more.

### 3.7 | The cathode plus screen grid coupling: calculations

In circuits 4 to 8 of figure 3.2.1 different combinations of cathode and screen grid coupling are used. The cathodes are connected in such a way to the special transformer winding that there is negative feedback. This can be understood as follows (see figure 3.1.3).

When the voltage  $V_{g1}$  increases, then the anode voltage  $V_{a1}$  decreases. As a result of the phase connection of the cathode winding, the cathode voltage  $V_k$  will increase. This means that the voltage  $V_{g1k}$  between the control grid and the cathode increases less than the voltage between the control grid and the ground. Consequently, the effective amplification will be reduced, which is a characteristic of negative feedback. In circuit 4 to 8 of figure 3.2.1 the cathode negative feedback stands central.

At the screen grid connection the situation is different. In figure 3.2.1-4 as a consequence of the phase of the voltage on the screen grid, after an increase of  $V_{g1}$ , the voltage of the screen grid  $V_{g2}$  will increase even more with the result that the current flowing through the valve will increase as well. This is the same as positive feedback.

The same is valid for figure 3.2.1-5, but then the positive feedback, as compared to circuit 4, is reduced. In figure 6 the screen grid has a constant DC voltage; thus there is no positive or negative feedback.

With circuit 7 and 8 the screen grid voltage will, by an increase of  $V_{g1}$ , counteract the current increase through the valve, so that in this case we have a screen grid with negative feedback.

The systematic setup of the circuits in figure 3.2.1 shows that all possible useful combinations of screen grid and cathode coupling have been dealt with (except for cathode positive feedback as this will very easily give rise to oscillations and a very high internal resistance of the power valves where high end applications become less obvious). In the following paragraphs the properties of circuit 4...8 will be discussed in more detail.

For the determination of the characteristics and the properties of the amplifier circuits, a procedure must be defined first that will enable the maximum scope to



be determined where the control grid voltage can vary up to the maximum driving range.

If in the case of circuit 1 to 3, it could be clearly determined that the control grid voltage had to vary between 0 and  $-72.4$  V, now, as a result of the cathode negative feedback, the control grid voltage  $V_{g1}$  would have a much broader range.

In formula 3.1.2  $V_{g1k-1}$  is made equal to 0 V: the situation of the maximum driving range of valve-1. For valve-2 then  $V_{g1k-2}$  must be equal to  $-72.4$  V (see formula 3.1.3). Subsequently, with the aid of formulas 3.1.9 and 3.1.11 the extreme  $\delta I_{\text{eff}}$  values (maximum drive applied) will be calculated and the intersection of this line with the  $1/4 \cdot Z_{aa}$  load line will be determined. This then will result in the maximum anode voltage variation in respect to  $V_{a0}$ .

Subsequently, with the aid of the given  $\Gamma$ -value the maximum variation of the cathode voltage can be determined. This maximum variation gives, in combination with the known variation of  $V_{g1k}$ , the range of the control grid  $V_{g1-1}$  (and the reverse of  $V_{g1-2}$ ) which has to vary in order to drive the valve to its limits. This range will subsequently be divided into ten equal steps ( $\delta$ ) whereby the control grid voltage  $V_{g1}$  can, in the calculations, be gradually varied.

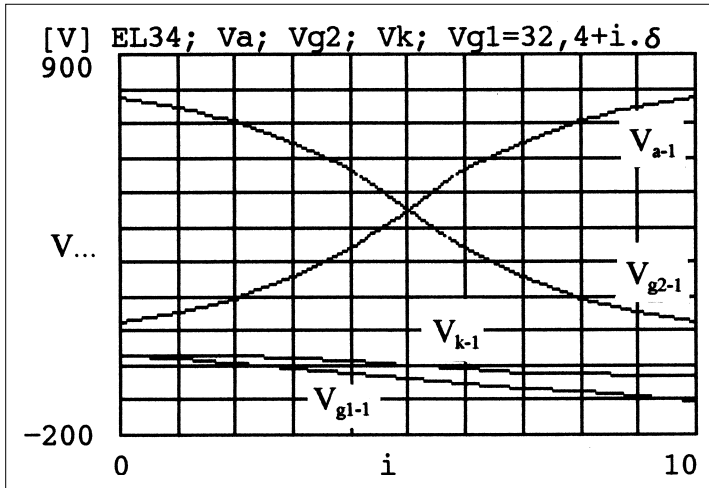
This procedure ensures that the input voltage varies linearly, whereby the possible distortion in the effective output voltage of the amplifier setup becomes clearly visible.

Here we must emphasise, however, that the characteristics obtained in this manner are the *dynamic* representations of the characteristics of the real momentary currents and voltages that occur in an amplifier when amplifying alternating voltages.

### 3.8 | $\Gamma = 0.1$ -cathode negative feedback, $x = -1$ -screen grid positive feedback

The underlying idea for this remarkable amplifier (see figure 3.2.1) is as follows: because of the cathode negative feedback the internal resistance of the power valves is greatly reduced, which is favourable for a larger damping of the speakers connected to the amplifier. The cathode negative feedback pushes the curves closer together, which reduces the maximum output power. By using a certain amount of the screen grid positive feedback the curves can be pulled apart again, we may expect that there is an increased amount of power output available.

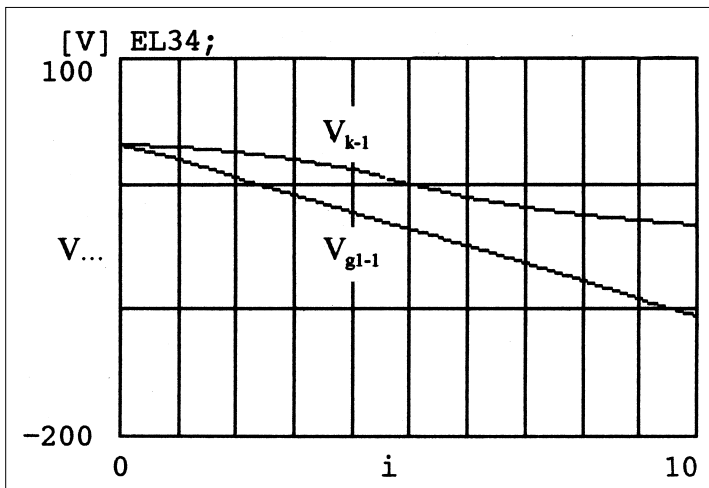
Figure 3.8.1 shows the various voltages of valve-1 and there it is shown clearly that by an increase of  $V_{g1}$  the screen grid voltage  $V_{g2}$  also increases, the amplification decrease caused by the cathode negative feedback is partially compensated for. In this graph  $\delta$  has a value of  $-13.73$  V.



↑ **Figure 3.8.1** The element voltages of valve-1.  $i$  runs from 0 to 10 with  $V_{g1} = 32.4 - i \cdot 13.73$  [V].

Conforming to the procedure of the previous paragraph:  $V_{g1} = 32.4 + i \cdot (-13.73)$  [V] whereby  $i$  runs from 0 to 10. As in the previous paragraphs  $i = 5$  represents the idling position with  $V_{g1} = -36.3$  V (see paragraph 3.3 with  $I_{a0} = 45$  mA).

Figure 3.8.2 shows the screen grid and the cathode voltages of valve-1 in detail. Both figures 3.8.1 and 3.8.2 show very clearly that the linearity of this amplifier is extremely poor indeed. The anode voltages most certainly are not linear with the control grid voltages and because of the character of the non-linearity there is a large amount of third harmonic distortion (symmetrical limitation).

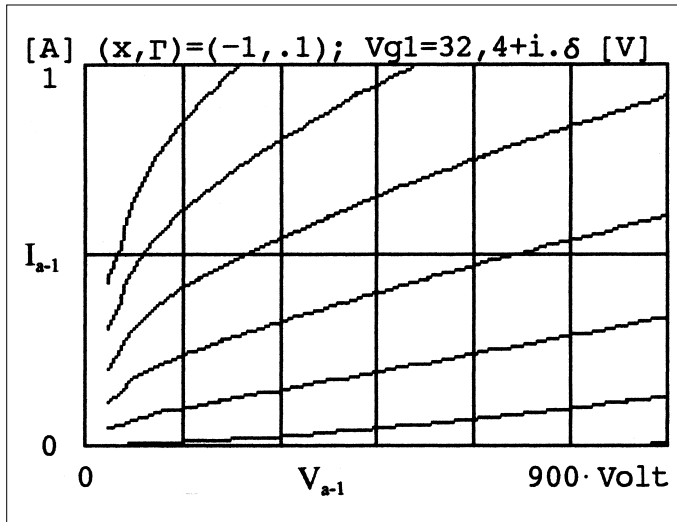


↑ **Figure 3.8.2** The control grid and cathode voltages.

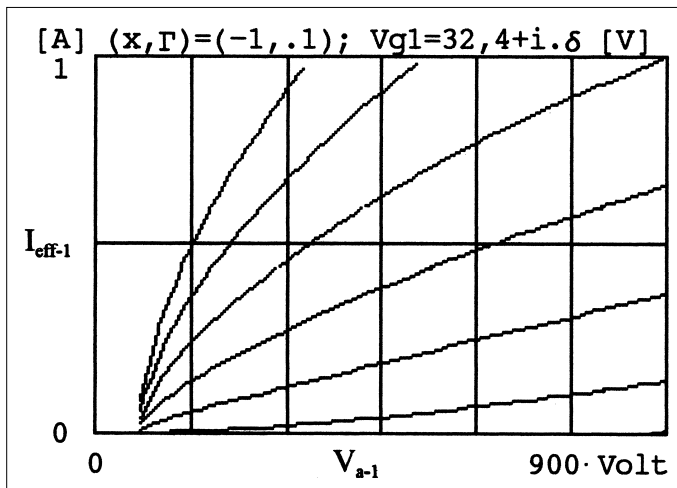


The non-linearity of the anode voltage is fed back to the cathode voltage (via the output transformer) which likewise exhibits a strong non-linearity. The difference of the screen grid voltage and the cathode voltage effectively drives the power valves; within this circuit there will be a large amount of distortion.

Figure 3.8.3 shows the anode current characteristics: it is striking (as predicted) that the leftmost line, which belongs to  $V_{g1k} = 0 \text{ V}$  ( $i = 0$ ), ended up far to the left and high up in the characteristic. This points to a large output power potential.



↑ **Figure 3.8.3** The anode current characteristics.



↑ **Figure 3.8.4**  $I_{\text{eff}}$  of valve-1.

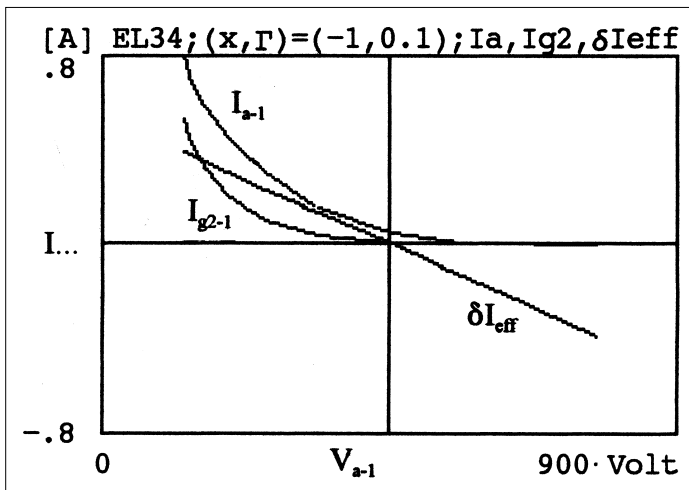


However in paragraph 3.2 we have seen that it is not just the anode current that drives the output transformer. The cathode current and the screen grid current contribute to the total effective magnetic flux density of the output transformer, resulting in an effective current  $I_{eff}$  per valve driving the output transformer (see formula 3.1.9). Figure 3.8.4 shows the effective current of valve-1; here it is striking that the outermost characteristic (for  $i = 0$ ) is now positioned much lower than in figure 3.8.3.

What is the causative factor? The cause is that the alternating current through the screen grid winding is, as seen from a magnetic perspective, opposed to the anode alternating current. Thus the screen grid current reduces the magnetic field rather than enhancing it. Therefore, effectively there is not much gain to be had for the output transformer. The situation is so bad (as shown in figure 3.8.5) that the anode and screen grid currents increase drastically and effectively work against each other with the result that only unwanted heat is produced.

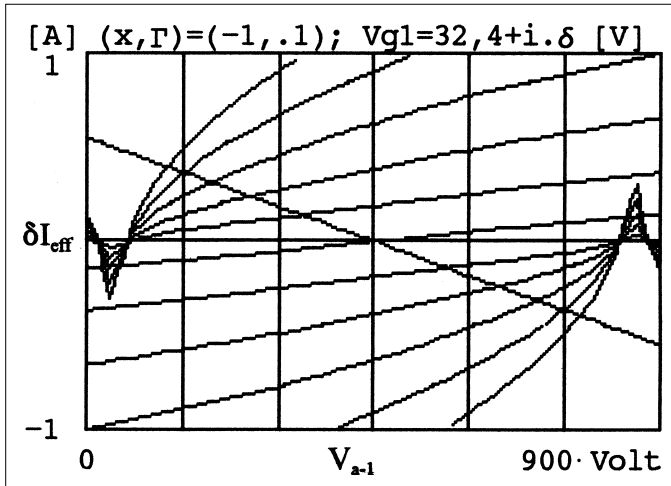
The previous proved itself by the premature aborted tests of this particular circuit. As well as the screen grid, the anode started to glow brighter through an increase of the output power, while the ripple voltage on the rectified power supply increased excessively because of the additional extra large current consumption via the anode and the screen grid.

Finally figure 3.8.6 shows the  $\delta I_{eff}$  characteristics and also the load line of the output transformer. This figure is extremely suitable to use alongside the procedures of paragraph 3.7 as the comparison will make it clear why the proposed procedure has been used to calculate the control grid voltage variations.



↑ Figure 3.8.5  $I_a, I_{g2}$  of valve-1 and  $\delta I_{eff}$





↑ **Figure 3.8.6**  $\Delta I_{\text{eff}}$  and the load line  $1/4 \cdot Z_{aa}$ .

Concluding: circuit 4 of figure 3.2.1 is an unsuitable combination of the screen grid positive feedback and the cathode negative feedback. The results are disappointing, a large amount of heat production of the power valves, a large amount of third harmonic distortion and a moderate amount of output power (about 64 W and only as long as the valves remain in one piece).

The outcome explains why for this circuit in the tables 3.2.1 and 3.2.2, no measured values have been reported.

### 3.9 | **G = 0.1-cathode negative feedback and $x = -0.33$ - screengrid-positive feedback: the Super Pentode circuit®©1**

The design philosophy of this circuit is as follows. The cathode negative feedback creates a reduction of the effective internal resistance of the power valves. (Although not within the scope of this paragraph there are some reasons to consider why it is desirable to have a low  $r_{i\text{-eff}}$ . First, the damping factor will become larger. Second, the frequency range of the output transformer will become larger too. Third, by an appropriate dimensioning of  $\Gamma$ , the distortion (THD) will decrease.) The screen grid positive feedback increases the 'driving range' of the amplifier.

In the amplifier discussed in the previous paragraph the amount of screen grid positive feedback was so large that the effective current that drove the output transformer became less than the anode current.

1) ® ©: Registered by and copyright of ir.buro Vanderveen 1996.

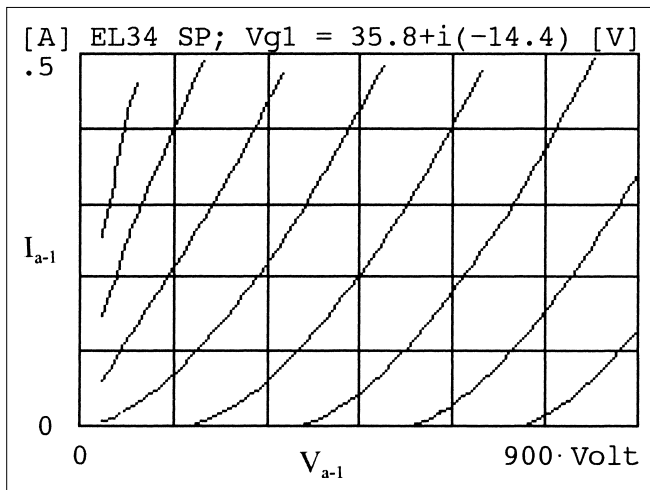


In regards to the efficiency this, then, is not a favourable situation. Formula 3.1.9 shows that if the second and the third part of the expression compensate one another (x and  $\Gamma$  contributions more or less abrogate each other) a limit situation has then been reached whereby the effective current strength and  $I_a$  are equal to one another.

Under those circumstances a balance can be sought-after whereby the characteristics of the power valves will be altered to the extent that a larger driving range becomes possible (the  $V_{g1k} = 0$  V line moves further to the left and upwards) while the current through the power valves does not increase excessively. In the amplifier circuit to be discussed this balanced situation has been approached.

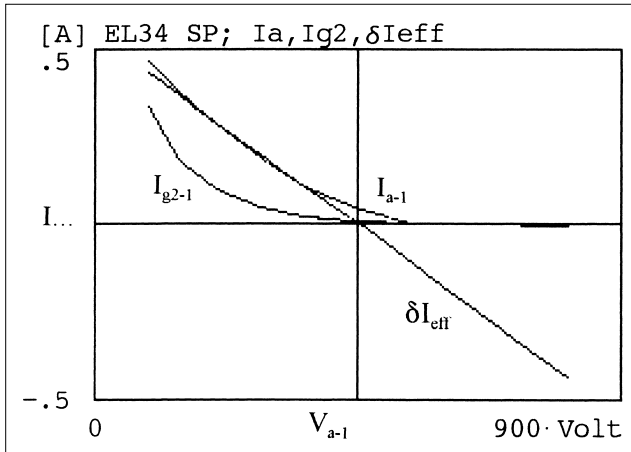
The above can be formulated differently: by increased control grid voltage the cathode voltage increases too (cathode negative feedback). By trying to find a position for the tap placement (x value) on the primary winding for the screen grid to be connected to, a situation can be reached where the screen grid voltage increases equally (or a tiny bit more) to the cathode voltage increase. Effectively the voltage difference between the cathode and the screen grid remains equal (or increases even a little).

The power valve, when amplifying an alternating voltage, will thus remain continuously in a pentode configuration whereby the voltage between the cathode and the screen grid does not alter. The driving range can be increased (a larger amount of output power is obtainable), while nevertheless the internal resistance of the power valves, because of the cathode negative feedback, is drastically reduced and is much smaller than the internal resistance of a 'pure' pentode power valve.



↑ **Figure 3.9.1**  $I_a / V_a / V_{g1}$  super pentode characteristics.



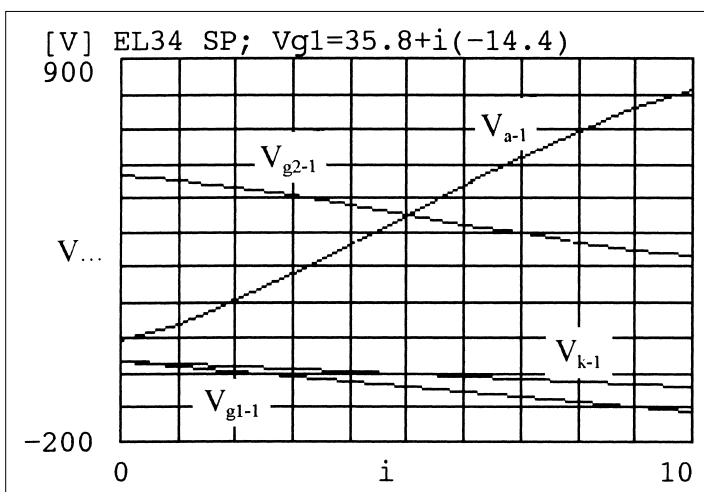


↑ **Figure 3.9.2**  $I_{a-1}$ ,  $I_{g2-1}$  and  $\delta I_{eff}$  as a function of  $V_{a-1}$ .

Because of these special properties this amplification circuit has been given its own name, namely the Super Pentode circuit. The name and the principle of it can be applied to those circuits where  $x \leq -\Gamma$  is valid with  $\Gamma > 0$ .

Figure 3.9.1 shows the anode current curves for  $V_{g1} = 35.8 - i \cdot 14.4$  [V]. The comparison, with figure 3.3.1 (pure pentode configuration) shows very clearly that the internal resistance is reduced (steeper slopes) while the driving range has been increased (the  $V_{g1k} = 0$  V line ( $i = 0$ ) lays further to the left and higher up).

Figure 3.9.2 shows the relations between the current of valve-1 and the effective current  $\delta I_{eff}$  that drives the output transformer. As predicted there is almost a complete overlap of the anode current and  $\delta I_{eff}$ .

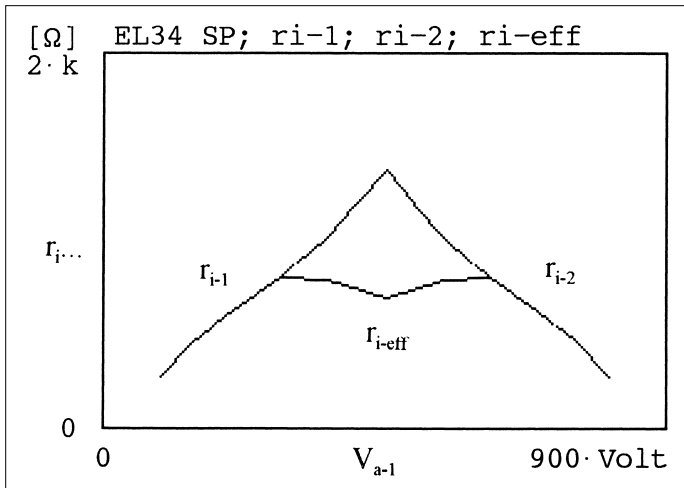


↑ **Figure 3.9.3** The valve voltages in a SP-configuration.

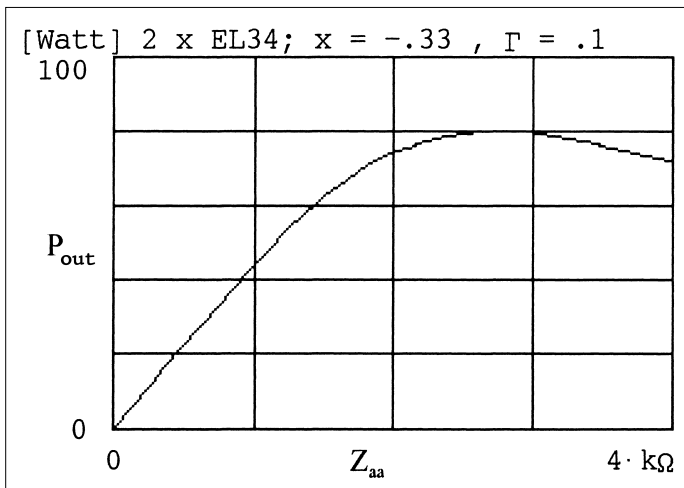


The interdependency between the various voltages on the various parts of the valve is shown in figure 3.9.3; it becomes clear that the anode voltages now vary linearly with the grid voltages. There is still some non-linearity, but this only happens when the valves have been driven close to their maximum. The type of non-linearity is such that it can be compensated for by an additional amount of overall negative feedback.

Figure 3.9.4 shows that within the class-A range the effective internal resistance  $r_{i-eff}$  remains almost constant. By a change over to a class-B situation  $r_{i-eff}$  will be reduced additionally. This situation is comparable to the pentode setup (compare with figure 3.3.5).



↑ **Figure 3.9.4** The internal resistances as a function of  $V_{a-1}$ .



↑ **Figure 3.9.5**  $P_{out}$  as a function of  $Z_{aa}$ .



Finally, figure 3.9.5 shows the maximum output power as a function of the impedance of the total primary winding. All tests and calculations happened with a  $Z_{aa} = 3.3 \text{ k}\Omega$ .

The following summary can be made about this particular amplifier setup.

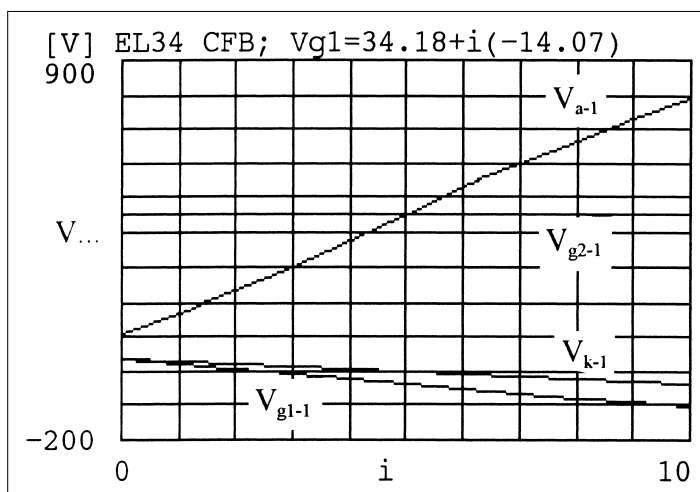
- 1 The output power is larger than with the 'pure pentode'.
- 2 The damping factor is comparable to a triode.
- 3 The overall efficiency is comparable to the 'pure pentode'.
- 4 The linearity of the anode and screen grid voltages is comparable or better than with the 'pure pentode'.

These remarkable properties justify the fact that this circuit received its own name.

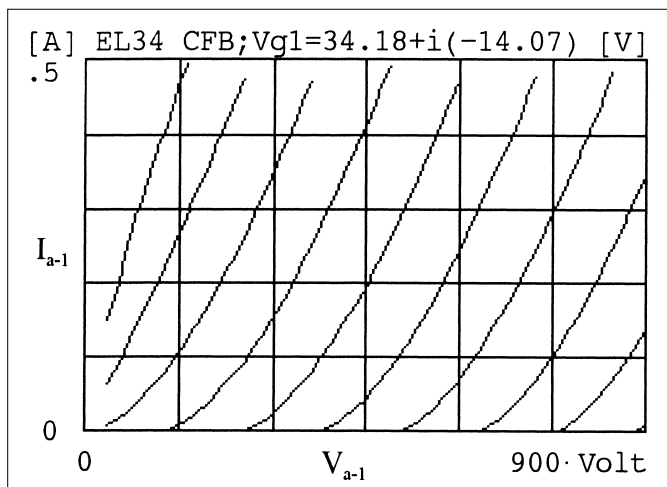
### 3.10 | $\Gamma = 0.1$ -cathode negative feedback: the CFB-circuit

The hallmark of circuit 6 of figure 3.2.1 is that the cathode exclusively creates negative feedback, while the screen grid is connected to a constant power supply. The name of this circuit points to the cathode negative feedback (CFB = *Cathode Feed Back*).

Figure 3.10.1 depicts the voltages on the different elements of the valve; it becomes clear that the voltage between the screen grid and the cathode is reduced by an increased  $V_{g1}$ . In reality, therefore, it is still a case of screen grid negative feedback, but in the literature there is little or no reference to it (see [1]).



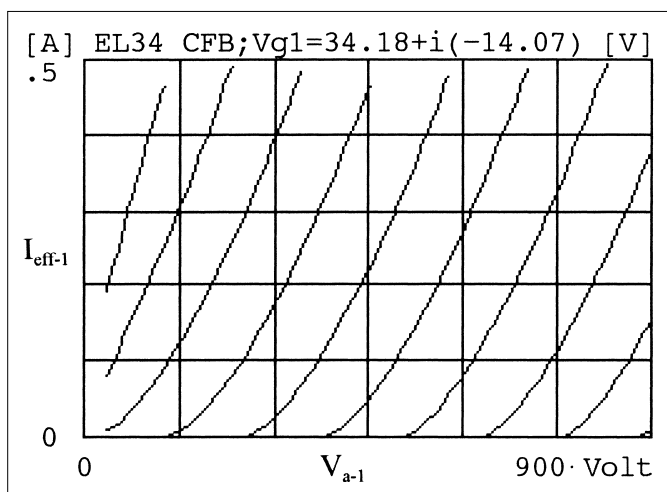
↑ **Figure 3.10.1** The valve voltages in a CFB-configuration.



↑ **Figure 3.10.2**  $I_a/V_a/V_{g1}$  CFB-characteristics.

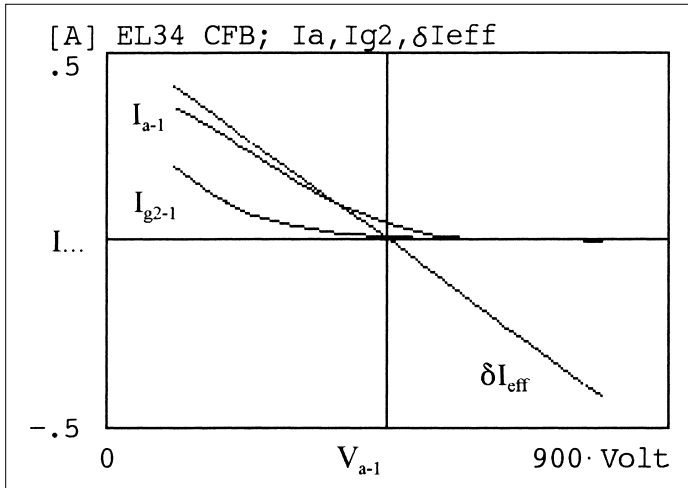
Figure 3.10.2 shows the  $I_a/V_a/V_{g1}$ -characteristics ( $V_{g1} = 34.18 - i \cdot 14.07$  [V]). Figure 3.10.3 shows the effective current characteristics of valve-1 (see formula 3.1.9) and it is striking that these are higher than the anode current characteristics. This is caused by the screen grid current that also flows through the cathode negative feedback winding and therefore effectively contributes to the magnetic flux density in the output transformer. See also figure 3.10.4.

If we compare in succession the circuits 4, 5 and 6 of figure 3.2.1 (paragraphs 3.8, 3.9 and 3.10), then it becomes clear that the super pentode circuit of paragraph 3.9 represents exactly that situation whereby  $\delta I_{eff}$  follows the behaviour of



↑ **Figure 3.10.3**  $\delta I_{eff}$ -characteristics.



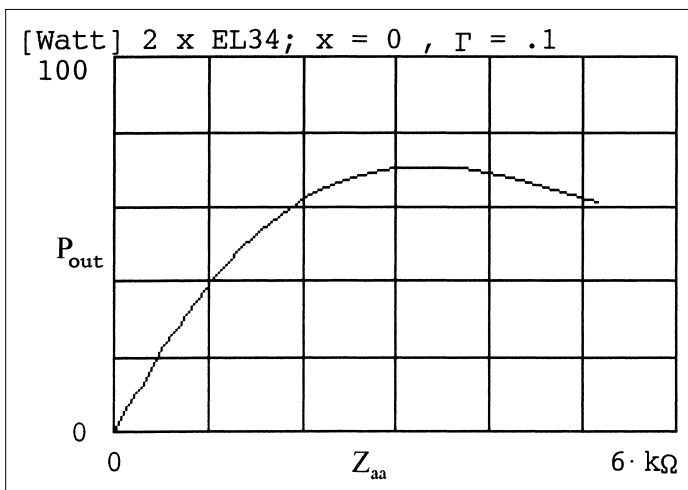


↑ **Figure 3.10.4**  $I_a$  and  $I_{g2}$  of valve-1, and  $\delta I_{eff}$

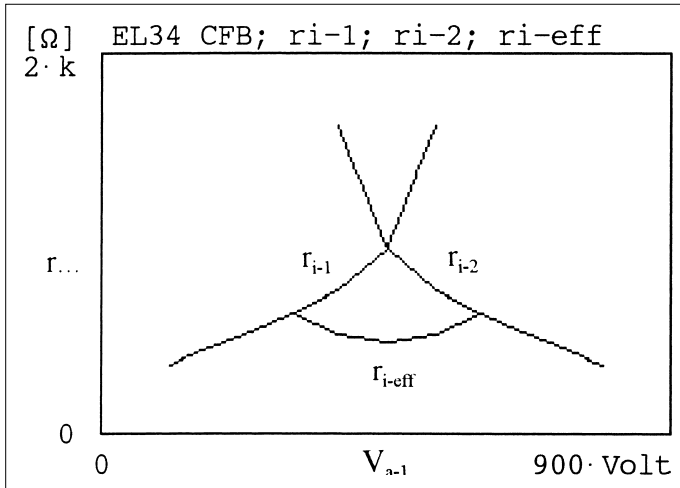
$I_a$ , while in paragraph 3.8  $\delta I_{eff} < I_a$  and in the CFB-circuit of this paragraph  $\delta I_{eff} > I_a$ .

The output power that can be delivered by this circuit (figure 3.10.5) is at its maximum with  $Z_{aa} = 3.3 \text{ k}\Omega$  and it is precisely with that impedance value that the measurements have been taken and the calculations have been done.

The behaviour of the internal resistances of the valves are finally shown in figure 3.10.6. Each of the properties of this concept are very good and in this regard it is not surprising that the renowned manufacturer Audio Research applies this circuit in its power amplifiers.



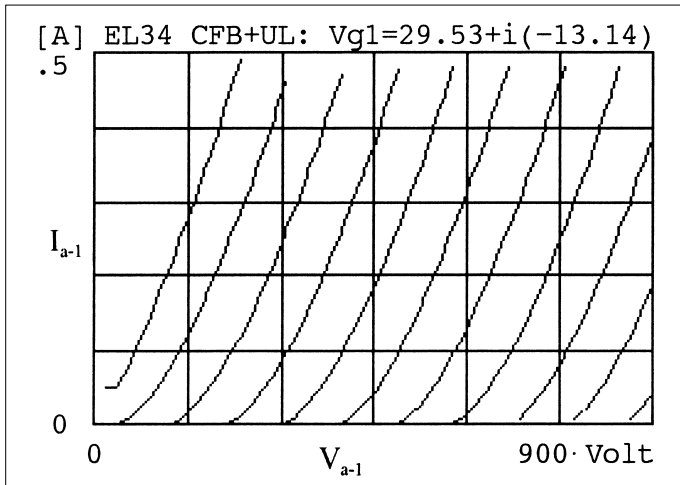
↑ **Figure 3.10.5**  $P_{out}$  as a function of  $Z_{aa}$ .



↑ **Figure 3.10.6**  $r_{i-1}$ ,  $r_{i-2}$  and  $r_{i-eff}$  as a function of  $V_{a-1}$ .

### 3.11 | $\Gamma = 0.1$ -cathode- and $x = 0.33$ screen grid negative feedback: the super triode circuit®<sup>1</sup>

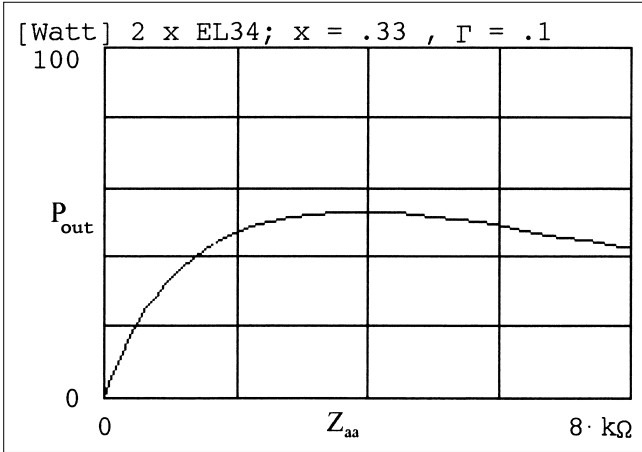
In circuit 7 of figure 3.2.1 negative feedback is applied to both the cathode and the screen grid. Because of this the  $I_a/V_a/V_{g1}$ -characteristics will be moved slightly to the right and the maximum output power will be reduced. With  $Z_{aa} = 3.3 \text{ k}\Omega$  this is equal to 53 W while for  $Z_{aa} = 4 \text{ k}\Omega$  the maximum output power has been obtained (see the figures 3.11.1 and 3.11.2).



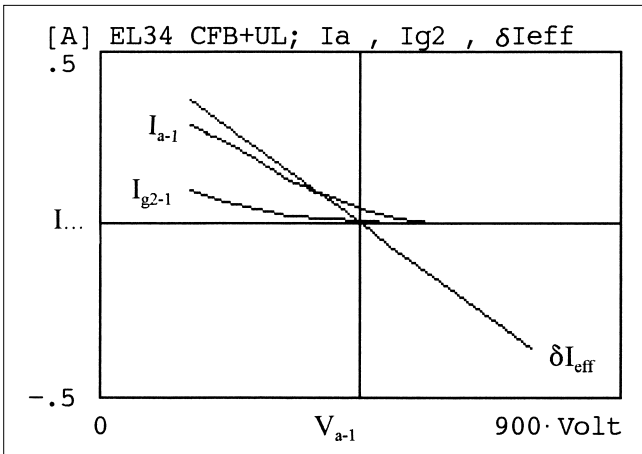
↑ **Figure 3.11.1**  $I_a/V_a/V_{g1}$  CFB and UL characteristics.

1) ©: Registered by and copyright of ir.buro Vanderveen 1996.





↑ **Figure 3.11.2**  $P_{out}$  as a function of  $Z_{aa}$ .



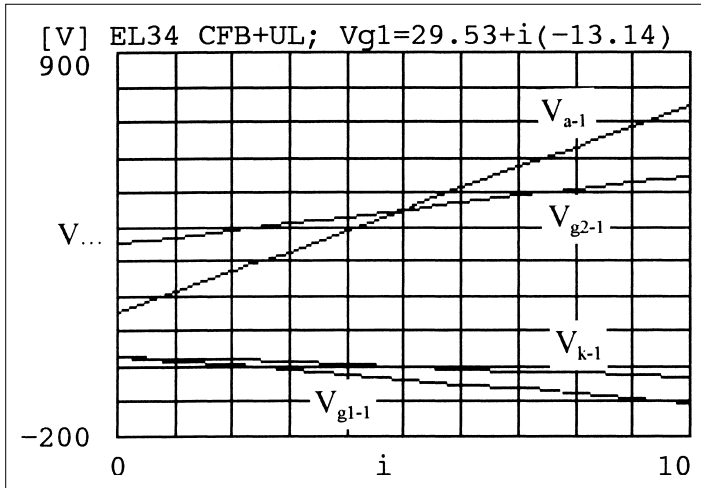
↑ **Figure 3.11.3**  $I_a$  and  $I_{g2}$  of valve-1, and  $\delta I_{eff}$

The effective current  $\delta I_{eff}$  is now even higher than  $I_a$  and the reason for that is that the screen grid current now effectively contributes to the flux density of the output transformer via the cathode negative feedback winding and the screen grid negative feedback winding. See figure 3.11.3.

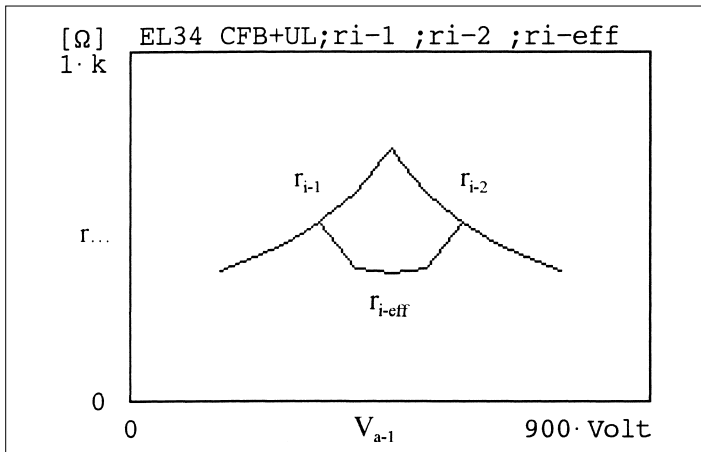
In comparison with the previous paragraphs the linearity of  $V_{g1}$  and  $V_a$  is has become even better (see figure 3.11.4).

The behaviour of the internal resistances has been drawn in figure 3.11.5.

Out of all these deliberations and results it follows that this concept moves the properties considerably closer to those of a triode power amplifier, while the output power is almost double of a standard triode based amplifier. That is why this topology has received its own birth name and is called the "Super Triode Circuit"<sup>®©</sup>.



↑ **Figure 3.11.4** Valve voltages in a CFB+UL-configuration.



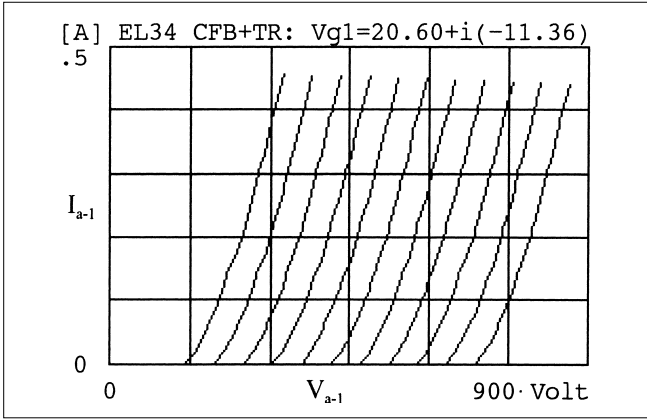
↑ **Figure 3.11.5**  $r_{i-1}$ ,  $r_{i-2}$  and  $r_{i-eff}$  as a function of  $V_{a-1}$ .

### 3.12 | $\Gamma = 0.1$ -cathode- and $x = 1$ screengrid negative feedback

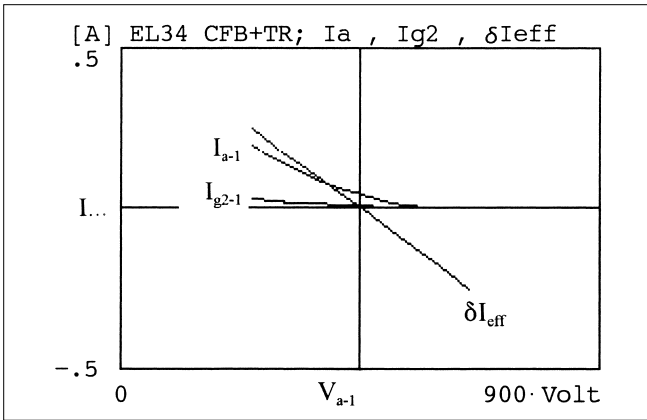
The last concept circuit being dealt with is circuit 8 of figure 3.2.1. The power valves are connected by means of the coupling of the screen grids to the respective anodes in a triode configuration. Via the cathode winding, cathode negative feedback has been used. The valve characteristics are being moved closely together and are showing very steep curves. The output power has been drastically reduced while the linearity between  $V_a$  and  $V_{g1}$  is exemplary.

The following figures show the properties of this particular circuit. The graph of the internal resistances shows a great resemblance to the behaviour of the in-

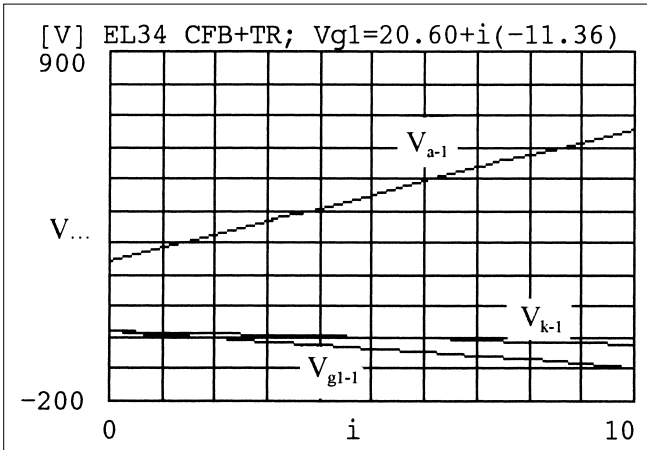




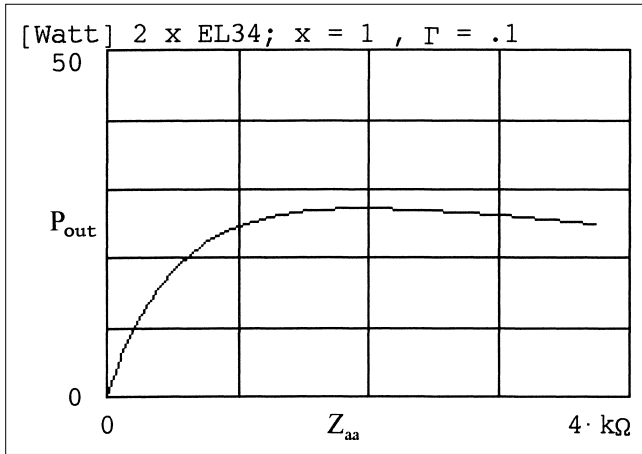
↑ **Figure 3.12.1**  $I_a / V_a / V_{g1}$  CFB and triode characteristics.



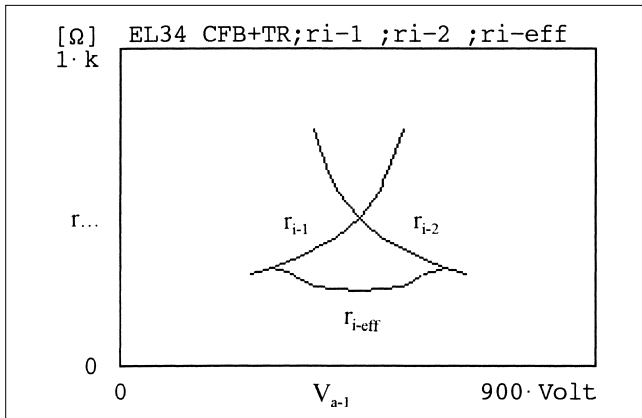
↑ **Figure 3.12.2**  $I_a$  and  $I_{g2}$  of valve-1, and  $\delta I_{eff}$



↑ **Figure 3.12.3** Valve voltages in a CFB and triode configuration.



↑ **Figure 3.12.4**  $P_{out}$  as a function of  $Z_{aa}$ .



↑ **Figure 3.12.5**  $r_{i-1}$ ,  $r_{i-2}$  and  $r_{i-eff}$  as a function of  $V_{a-1}$ .

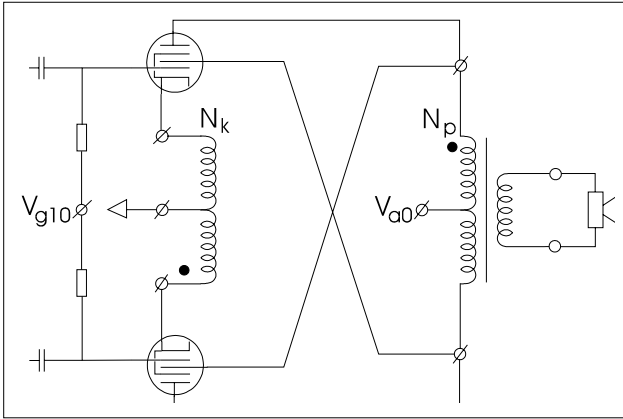
ternal resistances of a standard triode setup (see paragraph 3.5), and therefore lends itself to further optimisation as in paragraph 3.6.

The most important property of this CFB plus triode configuration, is above anything, that the internal resistances have been drastically reduced. This amplifier configuration is therefore extremely suitable when no negative feedback is applied (big linearity) while at the same time a large damping factor is required.

### 3.13 | The “Unity Coupled” circuit

About 1946 McIntosh introduced the Unity Coupled circuit. The hallmarks of this circuit are: a large damping factor, the power valves work almost completely within class-B and in the 2×EL34 setup an output power of 70 W is





↑ **Figure 3.13.1** The essence of the Unity Coupled circuit.

available. For further details see [1], [3], [4] and [5]. The essence of the Unity Coupled circuit is represented in 3.13.1

In the Unity Coupled setup  $N_k$  equals  $N_p$ . Using the language of the basic theory of paragraph 3.1, this means that  $\Gamma = 1$ . Since the screen grids are 'inversely' connected to the opposite laying anodes,  $x = -1$ . Using this method of connection ensures that when amplifying an alternating voltage, the voltage per valve between the screen grid and the respective cathode remains constant.

For each valve the cathode current  $I_k$  equals the anode current  $I_a$  and the screen grid current  $I_{g2}$ .  $I_k$  and  $I_a$  contribute to the magnetic field within the output transformer, while  $I_{g2}$  counteracts this field. Considering  $\Gamma = 1$  the effect of the counteraction of  $I_{g2}$  is compensated for in the  $I_{g2}$ -part in the cathode current. Effectively, only the  $I_a$ -contribution remains generating a magnetic field of  $1/2 \cdot N_p$  and  $1/2 \cdot N_k$  (per valve). That is why  $N_p$  plus  $N_k$  must be chosen in such a way that an optimum load for the EL34 power valves has been obtained.

In the next example the supply voltage of the EL34 is 450 V; in this situation an effective load of  $4000 \Omega$  is the optimum. Taking the above into consideration, the assumption of  $Z_{aa} = Z_{kk} = 1000 \Omega$  is valid.

The toroidal output transformer VDV1070-UC (= PAT-1070-UC) has been developed specifically for the application and the testing of this concept. Table 3.13.2 gives an overview of the calculated and measured results (see also [1]).

Within the calculations the 'old' EL34 parameters are used as introduced in paragraph 3.2.

The measured and calculated values overlap each other enough, the practical output power is somewhat lower. This is not due to the amount of idling current applied as this circuit has almost no sensitivity in regards to that. Apart from some uncertainty in the measurements the causative factor must be found in the insertion loss in the output transformer.



**Table 3.12.2 Calculated and measured values with 2x EL34, connected to the VDV1070-UC transformer**

<i>UC</i>	<i>Calculated</i>	<i>Measured</i>	<i>Unit</i>
$V_{a0}$	450	450	V
$I_{a0}$	45	42	mA
$V_{g10}$	-36,2	-38	V
$P_{\max}$	74	65	W
$r_{i\text{-eff}}$	55	67	$\Omega$
$f_{-3H}$	451	494	kHz

For the calculations of  $r_{i\text{-eff}}$ , use has been made of the valve parameters around the idling situation (see paragraph 3.2). Regarding this it must be said that the equivalent model that has been used here is completely described by figure 3.1.5. This means that the voltages, the currents and the internal resistances are acting upon the primary winding between the anodes of both the power valves, whereby  $Z_{aa}$  is equal to 1 k $\Omega$ . This is different to the approach in [1], where the internal resistances are considered to be in series with the anode and the cathode windings.

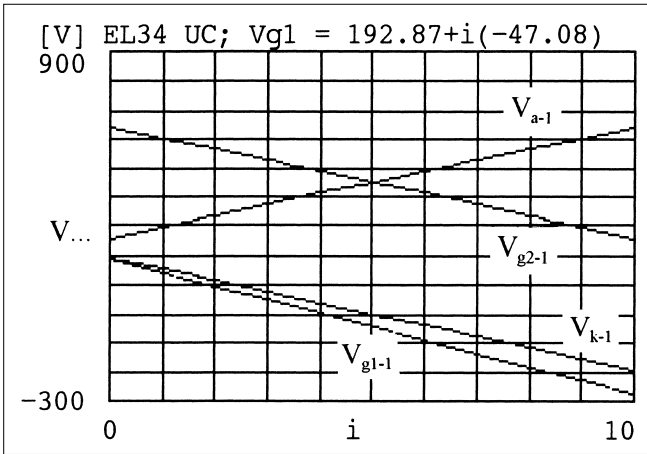
In regards to the  $f_{-3H}$ : this is the upper -3dB-frequency of the transfer function. In chapter 4 the calculation method will be further developed.

Below, the properties of the Unity Coupled circuit will be calculated in a situation where the operating point will be set with  $V_{a0} = 450$  V and  $I_{a0} = 5$  mA. This low idling current (almost the class-B range) gives none or almost no distortion as result of the large internal negative feedback. The screen grid voltage  $V_{g10}$  should, according to the idling current applied, be -42.5 V.

In order to drive the amplifier to its maximum the control grid voltage must be able to vary between 192.9 V and -278 V. In the following figures the control grid voltage is therefore represented by  $V_{g1} = 192.9 - i \cdot 47.08$  [V] with  $i = 0, 1, \dots, 10$ . The swing of the control grid is extremely large and the cause of that lies in the fact the voltage changes per valve on the cathode are equally as large as the voltage changes upon the anode. On top of that the control grid should have an additional voltage swing of  $0$  to  $2 \cdot (-42.5) = -85$  in respect of the cathode. With the experiments, the control grids were driven with the aid of a transformer with a windings ratio of 1:75 in order to realise the required large voltage swing. McIntosh has developed special driving circuits for the valves (see [3], [4] and [5]). A more detailed discussion is, however, outside the scope of this chapter.

Figure 3.13.2 gives a complete overview of the voltages on the various parts of valve-1. The large linearity between the various voltages, which points to a very minimal harmonic and cross-over distortion, is remarkable.



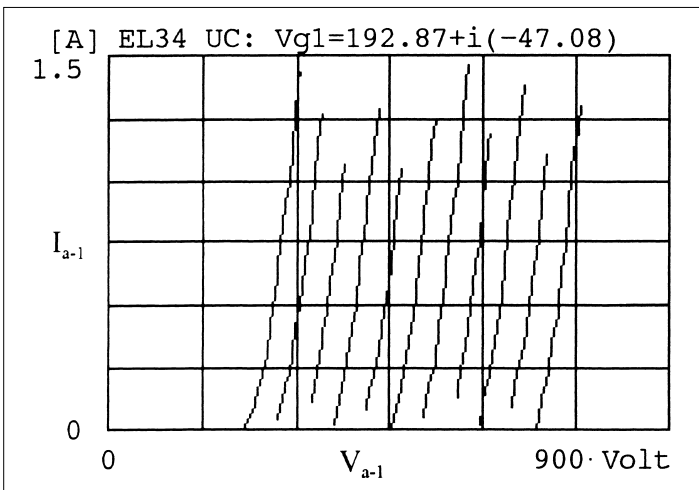


↑ **Figure 3.13.2** The voltages on the elements of valve-1 in UC configuration.

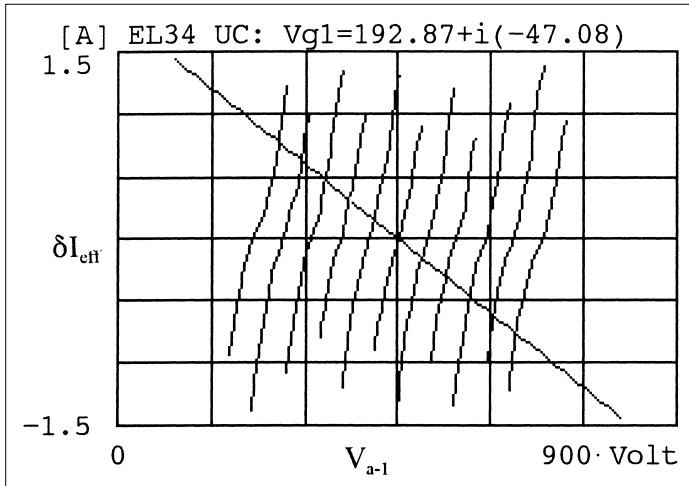
In figure 3.13.2 it is also clearly visible that the voltages between the cathode and the screen grid of each of the valves remain constant, which is a pointer to the 'pentode'-character of this kind of setup.

Figure 3.13.3 shows the anode current characteristics. It is clearly visible that the very large internal negative feedback has changed the characteristics in such a large way that these no longer in any way resemble the standard pentode characteristics. These are now very steep and have crept closer together along the horizontal axis.

The  $\delta I_{eff}$ -characteristics have been drawn together with the  $1/4 \cdot Z_{aa}$  line in figure 3.13.4. Note that when driven to its maximum the anode current increases only to 386 mA ( $\delta I_{eff, max} = 2 \cdot I_{a, max}$ ).



↑ **Figure 3.13.3**  $I_a/V_a/V_{g1}$ -characteristics.

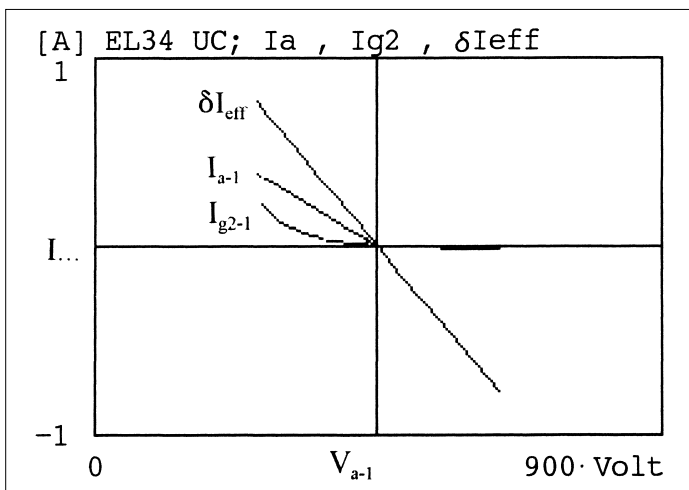


↑ **Figure 3.13.4**  $\Delta I_{eff}$  characteristics.

How the currents change when driven dynamically has been shown in figure 3.13.5. It is visible that  $I_{g2}$  does change, but it has no influence on  $\Delta I_{eff}$ . It is also recognisable that  $\Delta I_{eff}$  behaves itself as  $2 \cdot I_a$ . The valves operate almost completely in class-B but nevertheless  $\Delta I_{eff}$  shows not a kink in the zero pass region.

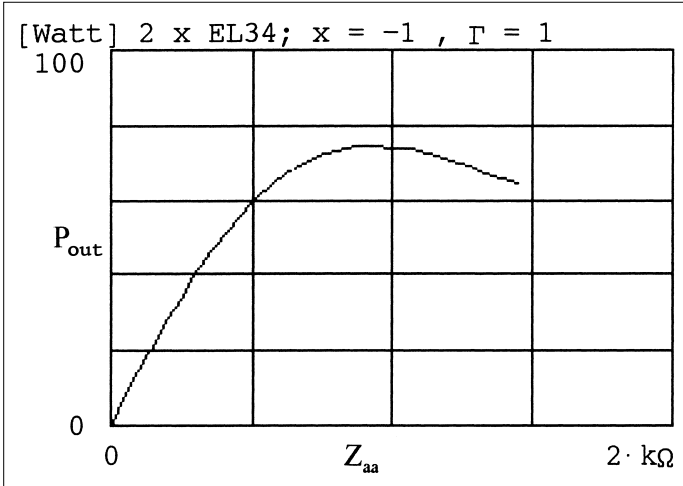
Figure 3.13.6 shows the output power as a function of  $Z_{aa}$ . It is noticeable that the output power is indeed (as predicted in the beginning of this paragraph) at its maximum when  $Z_{aa} = 1 \text{ k}\Omega$ .

In [1] two more circuit connections are being dealt with where the screen grids are respectively connected to the supply voltage  $V_{a0}$  ( $x = 0$ ) and to their



↑ **Figure 3.13.5**  $I_a$  and  $I_{g2-1}$  and  $\Delta I_{eff}$  as a function of  $V_{a-1}$ .



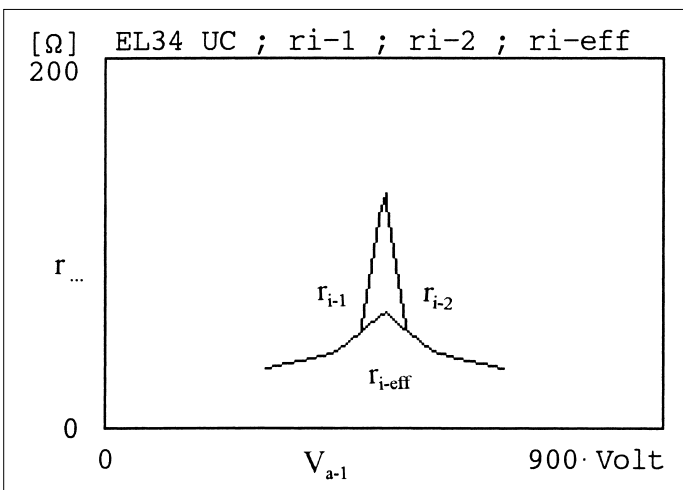


↑ **Figure 3.13.6**  $P_{out}$  as a function of  $Z_{aa}$ .

own anodes ( $x = 1$ ). Both the output powers will then be reduced to 43 W and 22 W respectively. Closer calculations of these conceptual circuits should be made as shown in previous paragraphs.

Finally, figure 3.13.7 shows the behaviour of the internal resistances and a further remark must be made here: around the setup point  $r_{i-eff}$  has reached its maximum. By increasing the idling current somewhat  $r_{i-eff}$  can then be adjusted in such a way that it remains constant around the setup point.

In conclusion, the following remarks can be made about the Unity Coupled circuit: the power stage has fantastical properties – a large linearity, a large



↑ **Figure 3.13.7**  $r_{i-1}$ ,  $r_{i-2}$  and  $r_{i-eff}$  as function of  $V_{a-1}$ .

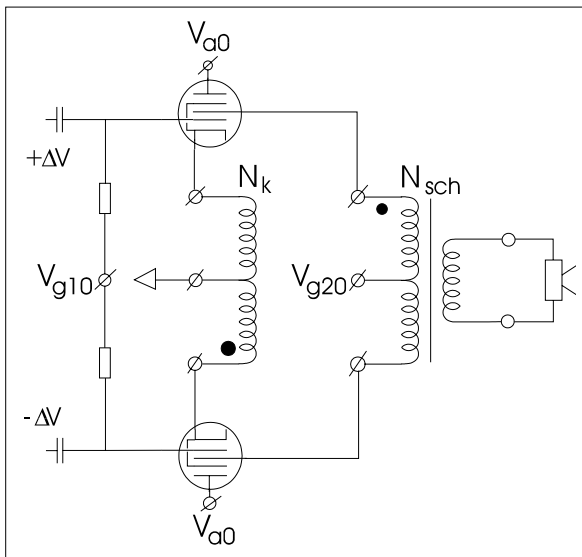


damping factor, safe maximum drive range of the power valves, minimal anode and screen grid dissipation and a large frequency range. The one drawback of this circuit is that an incredibly large driving voltage is required in order to drive the control grids into their maximum range. Maybe this also explains why, besides the question of patents and licenses, this amplifier has been reproduced so rarely and why the McIntosh valve amplifiers are still regarded to be very high end products.

### 3.14 | The cathode-follower push-pull end stage

There is a type of push-pull power amplification circuit that is not well described in the model defined in paragraph 3.1. We mean the setups whereby the anodes of the power valves are directly connected to the power supply  $V_{a0}$ . The cathodes are then coupled to the primary push-pull winding of the output transformer, the screen grids receive a fixed supply voltage  $V_{g20}$ , or are connected to a part-winding of the output transformer. By these so-called PPP-amplification-circuits the power valves will behave as cathode-followers.

The hallmark of the coupling model of paragraph 3.1 is that there are two variables present in the formulas:  $V_{a-j}$  and  $\Delta V$ . For each of the  $\Delta V$ -values, in the model, the associated  $V_{a-j}$  value is calculated, plus the associated current. In a PPP-setup that the anode voltage is constant and instead  $V_{k-j}$  varies as a function of  $\Delta V$ . This means that the model of paragraph 3.1 cannot describe the cathode-follower-circuit.



↑ **Figure 3.14.1** The concept schematic of the cathode-follower push-pull amplifier.



That is why we present you now with a new algebraic model for the cathode-follower push-pull end amplification setups. Figure 3.14.1 shows the concept schematic.

The mutual phase of the cathode and the screen grid windings has been marked with fat dots. The ratio of the screen grid and the cathode windings of the output transformer have been represented by formula 3.14.1.

Y is positive for the phase ratio as given in figure 3.14.1. If one changes the connections of the screen grid winding (the dot is then at the bottom) then Y will become  $-Y$  in the formulas below.

$$Y = \frac{N_{sch}}{N_k} \quad Y = 0 \quad (\text{in figure 3.14.1}) \quad (3.14.1)$$

Suppose that the momentary input voltage on the upper control grid capacitor of figure 3.14.1 is equal to  $\Delta V$ . The input voltage upon the bottom control grid capacitor will then be  $-\Delta V$ .

Suppose also that the momentary cathode voltage of valve-1 has been given by  $V_k$ . The corresponding voltages on each of the valve elements can be calculated with the aid of formulas 3.14.2 and 3.14.3.

$$\begin{aligned} V_{g1\ 1} &= V_{g10} + \Delta V \\ V_{k\ 1} &= V_k \\ V_{g1k\ 1} &= V_{g1\ 1} - V_k \end{aligned} \quad (3.14.2)$$

$$\begin{aligned} V_{g2\ 1} &= V_{g20} + Y V_k \\ V_{g2k\ 1} &= V_{g20} - Y V_k \\ V_{ak\ 1} &= V_{a0} - V_k \end{aligned}$$

$$\begin{aligned} V_{g1\ 2} &= V_{g10} + \Delta V \\ V_{k\ 2} &= V_k \end{aligned} \quad (3.14.3)$$

$$\begin{aligned} V_{g1k\ 2} &= V_{g1\ 2} - V_k \\ V_{g2\ 2} &= V_{g20} + Y V_k \end{aligned}$$



$$V_{g2k} = 2 V_{g20} Y V_k \quad V_k \quad (3.14.3)$$

$$V_{ak} = 2 V_{a0} V_k$$

For the calculation of the cathode current for each of the valves ( $j = 1, 2$ ) the Child-Langmuir equation can directly be applied without the aid of the  $\alpha_j$ -function defined in paragraph 3.1. This  $\alpha$ -function (see formulas 1.14.6 and 3.1.4) is only needed for the determination of the screen grid current.

Formula 3.14.4 shows for each valve, with the aid of formulas 3.14.2 and 3.14.3, the momentary cathode and screen grid currents can be calculated.

$$I_{kj} = K V_{g1kj} D_{g2} V_{g2kj} D_a V_{akj}^{1.5}$$

$$\alpha_j = \alpha_0 \frac{2}{\pi} \arctan \frac{V_{akj}^{\frac{1}{n}}}{V_{g2kj}} \quad (3.14.4)$$

$$I_{g2j} = 1 - \alpha_j I_{kj}$$

Following the model in paragraph 3.1 the flux densities generated by each of the cathode- and screen grid- currents within the core can now be calculated.

Subsequently for each valve- $j$ , an effective single cathode current that drives the  $1/2 \cdot N_k$  windings can be determined, and the 'magnetic' contributions of the cathode- and the screen grid- currents per valve combine (see formula 3.14.5).

$$I_{k\text{ eff }j} = I_{kj} \frac{1 - Y}{1 - \alpha_j} \quad (3.14.5)$$

Each of the valves- $j$  behave as a current source that delivers a momentary  $I_{k\text{ eff }j}$  with an internal parallel resistance that is represented by formula 3.14.6.

$$r_{ij} = \frac{\partial I_{k\text{ eff }j}}{\partial V_{kj}} \quad (3.14.6)$$

Considering that both the valves are set in a push-pull situation and their effective cathode currents, as seen from a magnetic perspective, are driven in an opposed manner through the effective primary cathode windings, all that remains is an effective difference current  $\delta I_{k\text{ eff}}$  that drives the  $1/2 \cdot N_k$  windings.

This current is defined by formula 3.14.7 while formula 3.14.8 delivers the respective effective internal resistance  $r_{i\text{ eff}}$ .



$$\delta I_{k \text{ eff}} = I_{k \text{ eff } 1} + I_{k \text{ eff } 2} \quad (3.14.7)$$

$$r_{i \text{ eff}} = \frac{1}{\frac{1}{r_{i 1}} + \frac{1}{r_{i 2}}} \quad (3.14.8)$$

These definitions are identical to the last phase of the model in paragraph 3.1. This means that the whole of the cathode-follower push-pull amplification circuit can now be replaced by a single current source  $I_{k\text{-eff}}$  that drives  $1/2 \cdot N_k$  windings paralleled by an internal current source resistance to the value of  $r_{i\text{-eff}}$  (see figure 3.1.4). Analogous to paragraph 3.1 the amplifiers can also be represented by a voltage source with a series resistance of  $4 \cdot r_{i\text{-eff}}$  driving a total of  $N_k$  windings, the voltage over the total cathode winding is  $(V_{k-1} - V_{k-2})$ , see figure 3.1.5.

The models as given in paragraphs 3.1 and 3.14 are now completely comparable. The application of the cathode-follower model is therefore identical to the results as given in paragraph 3.2 to 3.13. Further development will be left to the reader.

### 3.15 | Conclusion of chapter 3

Chapter 3 combines the results of chapter 1 and 2 to a single universal coupling model that describes the inter-action of the power valves and the output transformer in a push-pull amplifier.

Paragraph 3.1 gives a theoretical background of this coupling model, resulting in two equivalent approaches. The power amplifier can therefore be seen as a voltage or a current source with the respective internal series- or parallel-resistances.

Paragraph 3.2 gives an account of an investigation of the validity of the couplings model with the aid of comparisons of calculations and measurements of eight trial amplification configurations.

In the paragraphs 3.3 to 3.12 each of those trail amplifiers is discussed in detail and their characteristic properties have been derived. Additionally in paragraph 3.9 and paragraph 3.11 the new Super Pentode circuit<sup>®©</sup> and the Super Triode circuit<sup>®©</sup> are introduced. In paragraph 3.13 the coupling model has been applied to the 'Unity Coupled' configuration.

Finally, in paragraph 3.14 the theory of another coupling model has been presented for the 'cathode-follower' push-pull amplifiers.



### 3.16 | Bibliography of chapter 3

- [1] Ir. Menno van der Veen; *Specialist Rinkern Uitgangstransformatoren; De Super-Pentode-Schakeling*<sup>®</sup>; Januari 1997; Amplimo BV
- [2] Ir. Menno van der Veen; *Het Vanderveen Buizenbouwboek*; 6<sup>e</sup> druk; Amplimo BV
- [3] P.G.Sulzer; *Survey of Audio-Frequency Power-Amplifier-Circuits*; Audio Engineering; May 1951
- [4] R.F. Scott; *Circuit Features of High-Fidelity Power Amplifiers*; Radio Electronics; Aug. 1955; pp. 44–46
- [5] N.H. Cowhurst; *Realistic Audio Engineering Philosophy*; Audio; Oct. 1959
- [6] Ir. Menno van der Veen; *Modelling Power Tubes and their Interaction with Output Transformers*; 104th AES Convention; Amsterdam 1998; preprint 4643
- [7] Pierre Touzelet, Menno van der Veen; *Small signal analysis for generalized push-pull tube amplifier topology*; 112th AES Convention; Munich 2002; paper 5587

®©: The *Super Pentode circuit* and the *Super Triode circuit* are registered and under the copyright of Menno van der Veen. The concept of these circuits and the names are subjected to the copyright laws of the Netherlands and the European Union. Reproduction and production are worldwide not permitted. Requests for license must be directed to ir. Menno van der Veen. For contact details see the colophon page of this book.

